Numerical Investigation of loaded and unloaded diffuser equipped with a flange

Farouk Owis[a], M .T. S. Badawy[b], K. A. Abed[b], H. E. Fawaz[b], Amr Elfeky[b]

[a]Aerospace Dept., Faculty of Engineering, Cairo University, Egypt.
[b]Mech. Eng. Dept., National Research Center, Dokki, Cairo, Egypt.

Abstract—Numerical investigations were carried out for flow fields of a flanged diffuser wind turbine. Influence of expansion angle, diffuser length, flange height and load factor on the flow field described by velocity contours, static pressure contours and streamlines was investigated. A commercial package "ANSYS FLUENT 14.5" is used as a solver, while Gambit program is used for constructing the problem domain and mesh generation. The results showed that increasing the expansion angle leads to accelerate the flow through the diffuser when the angles are between 0° and 12° where the flow field is characterized by undisturbed streamline flows, after that the expansion angle effect become negligible as the secondary fluid circulation is generated near the end of the diffuser and grow with expansion angle. Also increasing the diffuser length accelerates the flow entering the diffuser until the diffuser length to inlet diameter ratio reaches a value of 1.25. After that, a recirculation zone is formed at the end of the diffuser. A high pressure region is formed in front of the diffuser flange and a low pressure region is generated behind it. The intensity and area coverage of these regions increase with flange height which leads to increase the overall flow speed inside the diffuser till flange height to diffuser inlet diameter ratio reaches to 0.75, it is found that by increasing the load factor C_t the acceleration factor decreases until reached to a value of C_t equal to 0.95, at this value of the load factor the acceleration factor still > 1. In another word the designed diffuser is still effective and able to increase the air velocity passing through it. By increasing C_t more than 0.95 the diffuser will not be effective in increasing the velocity passing through it and the acceleration factor will be lower than 1. also it is concluded that the best diffuser load is estimated to be in the range of 0.4 to 0.95.

Keywords—Flanged Diffuser; Wind Turbine; Load Factor; Output Power; diffuser angle; diffuser legnth; diffuser flange

1 INTRODUCTION

The limitation of fossil fuels is clear and the security of alternative energy sources is an important subject. Driven by an increasingly energy hungry world and a push towards sustainable. The development and application of renewable and clean new energy are strongly expected. Among others, wind energy technologies have developed rapidly and are about to play a big role in a new energy field. However, in comparison with the overall demand for energy, the scale of wind power usage is still small; especially, the level of development in Egypt is extremely small. As for the reasons, various causes are conceivable. For example, the limited local area suitable for wind power plants, and the turbulent nature of the local wind are pointed out. Therefore, the introduction of a new wind power system that produces higher power output even in areas where lower wind speeds and complex wind patterns are expected is strongly desired. The Flanged Diffuser Augmented Wind Turbine (FDAWT) was thought to provide such an opportunity, the concept of which entailed surrounding a wind turbine rotor with a duct that increased in cross sectional area downstream of the blade-plane. And large flange is attached to the outer periphery of a duct exit. The power (P) in wind is well known to be proportional to the cubic power of the wind velocity (U) approaching the wind turbine as follows:

$$P = \frac{1}{2}\rho A U^3 \, Cp \quad (1)$$

Nomenclature	
A	rotor area
Cp	pressure coefficient
Cp*	input power coefficient
Cp_b	base pressure coefficient
Cp_d	pressure recovery coefficient
C_t	load factor
D	diffuser diameter
h	flange height
k	turbulent kinetic Energy
K	acceleration factor
L	diffuser length
P	power generated
p	static pressure
U	wind velocity
Greek letters	
μ	molecular viscosity
μ_τ	turbulent viscosity
ε	turbulence dissipation rate
Φ	diffuser expansion angle
ρ	air density
Subscripts	
∞	Atmospheric
1	wind turbine inlet
2	wind turbine exit
b	diffuser exit

Where A, ρ and C_P are the rotor area, air density and pressure coefficient respectively. This means that even a small amount of acceleration gives a large increase in the energy output. Therefore, many research groups have tried to find a way to accelerate the approaching wind effectively using FDAWT. After the Second World War the idea of the attachment of a diffuser to a wind turbine was presented (Glauert (1959), Kogan and Seginer (1963), Oman and Foreman (1975)). Based on this idea, a group in New Zealand developed the Vortec 7 DAWT (Phillips et al.(1999), Phillips et al.(2000)) They used a multi-slotted diffuser to prevent separation within the diffuser. Also a diffuser shaped surrounding a wind turbine have been developed by Ohya et al. (2002) and Ohya et al. (2004). Abe and Ohya (2004) carried out a numerical investigations for flow fields around flanged diffusers to develop small-type wind turbines under 1.5 kW. and they suggested that the loading coefficient for the best performance of a flanged diffuser is considerably smaller than that for a bare wind turbine. At the small scale, Toshiaki Setoguchi et al. (2004) had performed a two-way diffuser with three types of outside body shape and three kinds of brim height. Toshio Matsushima (2006) evaluated a wind turbine fitted with a diffuser with the aim of improving the turbine's output power characteristics. he used thermohydrodynamic analysis software to simulate the effect of the diffuser parameters on the wind speed, and evaluated the turbine characteristics using a field trial device. Also Wang et al. (2008) developed an efficient small domestic wind turbine with a scoop. Yuji Ohyaa et al. (2008) have developed a diffuser wind turbine that can obtain a remarkably higher power output compared to conventional wind turbines. Then a flange of proper height is attached to the outer periphery of the diffuser exit, successfully realizing a remarkable increase in wind speed. Buyung Kosasih and Andrea Tondelli (2012) study the effects of diffuser geometry and presents the performance comparison of bare and shrouded geometry (diffuser, nozzle-diffuser, and brimmed diffuser). Chen et al. (2012) studies the flanged diffuser's effects on rotor performance of small wind turbines with rotor solidities between 20% and 60% at wind speeds between 10 m/s and 20 m/s. Kazuhiko Toshimitsu et al. (2012) developed a turbine with a flanged-diffuser shroud with high performance. They proved that the diffuser wind turbine has higher efficiency than the free wind turbine. They made an experimental and numerical investigation using CFD and Particle image

velocimetry (PIV) in steady wind at the flow structure around the compact-type wind turbine. Kardous et al. (2013) made a Numerical simulations, Particle-Image-Velocimetry visualizations and wind tunnel experiments to get a better understanding of the effect of the flange height on wind velocity increase at the inlet section of an empty flanged diffuser. CFD calculation was done by Kamyar Mansour and Peyman Meskinkhoda (2014) for flow fields around flanged diffusers to study small-type wind turbines. Their results showed that the wind turbine equipped with a flange and inlet diffuser shroud was demonstrated by realizing remarkable increase in wind speed of 1.6 – 2.1 times that of the approaching wind speed, therefore the power augmentation for a given turbine diameter and wind speed was increased by a factor about four compared to a standard (bare) wind turbine.

In the present paper, a detailed numerical investigation of the flanged diffuser geometrical parameters such as diffuser expansion angle, diffuser length and flange height on the flow field inside and around a flanged diffuser is carried out and a parametric study is performed to determine the optimum flanged diffuser geometry in order to develop a wind power system capable of collecting and accelerating the approaching wind. Also the load factor effect is studied in detail in order to obtain the acceptable range of load factor values in which the designed diffuser is effective and able to increase the air velocity passing through it.

2. MATHEMATICAL MODEL AND GOVERNING EQUATIONS

The numerical solution of fluid flow problem requires the solution of general equations of fluid motion, the continuity and Navier-Stokes equations described mathematically by these equations, which are a set of non linear partial differential equations with appropriate boundary conditions. In the following analysis, the Reynolds-Average-Naviaers–Stokes (RANS) equation is considered with renormalization group k-ε turbulence model, which are indicated in mass and momentum and can be expressed as follows:

Continuity:

$$\frac{\delta}{\delta x_i}(\overline{\rho U_\imath}) = 0 \tag{2}$$

Momentum:

$$\frac{\delta}{\delta x_j}\left(\overline{\rho U_\imath U_\jmath}\right) = -\frac{\delta \bar{p}}{\delta x_i} + \frac{\delta}{\delta x_j}\left[\mu_\tau\left(\frac{\delta \overline{U_\imath}}{\delta x_j} + \frac{\delta \overline{U_\jmath}}{\delta x_j} - \frac{2}{3}\delta_{ij}\frac{\delta \overline{U_\imath}}{\delta x_j}\right)\right] + \frac{\delta}{\delta x_j}\left[-\rho\overline{U_\imath' U_\jmath'}\right] \tag{3}$$

Where $\bar{p}$ is the mean pressure, $\bar{u}$ is the mean velocity, μ_τ is the molecular viscosity, and $-\rho\overline{u_\imath' u_\jmath'}$ denotes the Reynolds stress. To correctly account for turbulence, Reynolds stress is modeled utilizing the Boussineq hypothesis to relate the Reynolds stress to mean velocity gradients within the flow. The Reynolds stress is defined as:

$$-\rho\overline{U_i' U_j'} = \mu_\tau\left[\frac{\delta \overline{U_\imath}}{\delta x_j} + \frac{\delta \overline{U_\jmath}}{\delta x_i}\right] - \frac{2}{3}\left[\rho k + \mu_\tau \frac{\delta \overline{U_\imath}}{\delta x_i}\right]\delta_{ij} \tag{4}$$

Where μ_τ is the turbulent viscosity and k is the turbulent kinetic energy. For k-ε turbulence model the turbulent viscosity is computed through the solution of two transport equations for turbulent kinetic energy and turbulence dissipation rate ε. The RNG transport equations are:

$$\frac{\partial g}{\partial t}(\rho k) + \frac{\partial}{\partial x_i}(\rho k \overline{U_\imath}) = \frac{\partial}{\partial x_j}\left[\alpha_k \mu_{eff}\frac{\partial k}{\partial x_j}\right] + G_k + G_b - \rho\varepsilon - Y_M + S_k \tag{5}$$

$$\frac{\partial g}{\partial t}(\rho\varepsilon) + \frac{\partial}{\partial x_i}(\rho\varepsilon \overline{U_\imath}) = \frac{\partial}{\partial x_j}\left[\alpha_k \mu_{eff}\frac{\partial \varepsilon}{\partial x_j}\right] + c_{1s}\frac{\varepsilon}{k}(G_k + C3sGb - C2s\rho\varepsilon 2k - Rs + Ss \tag{6}$$

$$R_s = \frac{C_\mu \rho \eta^3 \left(1 - {}^{\eta}/_{\eta_0}\right)}{1 + \beta\eta^3}\frac{\varepsilon^3}{k} \tag{7}$$

The Load factor C_t states the pressure drop of the diffuser and in fact demonstrates the effect of replacement of the rotor by volume force, it is defined as the ratio of pressure drop caused by the wind turbine to the dynamic pressure at the turbine exit and is calculated through Eq. 8

$$C_t = \frac{p_1 - p_2}{(0.5\ \rho\ U_2^2)} \quad (8)$$

Rotor inlet air speed to the free stream air flow speed ratio is called acceleration coefficient (K) and is given by Eq. 9

$$K = \frac{U_1}{U_\infty} \quad (9)$$

Another parameter affecting the performance of a wind turbine with a diffuser is the input power factor Cp* which has a direct relationship with load factor as expressed in Eq. 10.

$$Cp^* = C_t K^3 \quad (10)$$

Base pressure coefficient Cp_b shows the total air pressure drop through the diffuser with turbine and is calculated by Eq. 11.

$$Cp_b = \frac{p_b - p_\infty}{(0.5\ \rho\ U_\infty^2)} \quad (11)$$

The pressure recovery coefficient Cp_d shows the pressure drop within the diffuser and is obtained through Eq. 12.

$$Cp_d = \frac{p_b - p_2}{(0.5\ \rho\ U_2^2)} \quad (12)$$

3. NUMERICAL METHOD AND COMPUTATIONAL CONDITIONS

The diffuser computational domain with its boundary conditions is shown in Fig. 1. The inlet boundary was set as the uniform flow velocity, the outlet boundary was set as pressure outlet, top was set as symmetry, because of less time for calculation and acceptable accuracy the bottom wall is set as axisymmetric. Load can be reprehensive by Porous jump condition that used to model known velocity (pressure-drop) characteristics. It is essentially a 1D simplification of the porous media model available for cell zones. A commercial package "ANSYS FLUENT 14.5" is used as a solver in which the finite volume method is used , while Gambit program is used for constructing the problem domain and mesh generation. The domain is drawn to cover the diffuser and it is extended 5D upstream and 8.5D downstream the diffuser with a height of 10 D. Structured grids of 165300 cells are used to discretize the computational domain. Grid points are clustered around the diffuser walls and the location of turbine as shown in figure 2. SIMPLE (semi-implicit method for pressure linked-equation) was used to links the velocity to the pressure in order to satisfy the continuity equation (to enforce mass conservation and to obtain the pressure field). A uniform wind speed of 5m/s is specified at the entrance of the domain. The study sets the flow as axisymmetric steady flow, segregated solver is proposed, and velocity formulation is absolute whereas the turbulence model is RNG k-ε model. Enhanced wall treatment function is chosen for the near wall treatment method, the turbulence intensity is 3%, momentum and turbulent kinetic energy is second order upwind with 10^{-6} of the convergence criterion.

4. RESULTS

4.1 Model validation

The present CFD model has been validated using experimental and numerical data of Abe and Ohya (2004) as shown in Figs 3, 4, 5 and 6 under different load conditions at diffuser expansion angle = 4°, diffuser legnth to diameter ratio =1.5, flange height to diameter ratio =0.5. Figures 3.a and 3.b show the on-axis distributions of streamwise velocity and pressure coefficient, respectively, of the present model and the experimental and numerical data of Abe and Ohaya (2004) with no load (C_t = 0). The present results show reasonable trends for both on-axis velocity and pressure variations. By comparing the results when the load factor C_t = 0.2 as shown in figure 4.a and 4.b

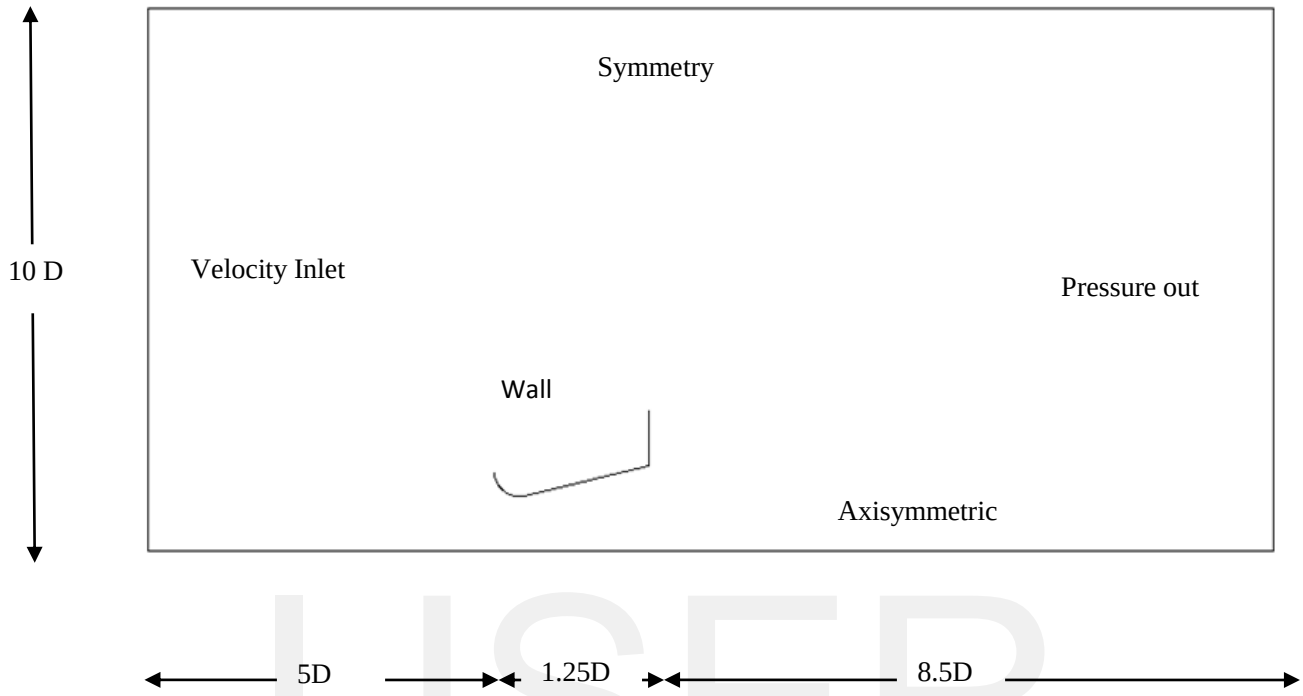

Fig. 1. Diffuser computational domain and the boundary conditions.

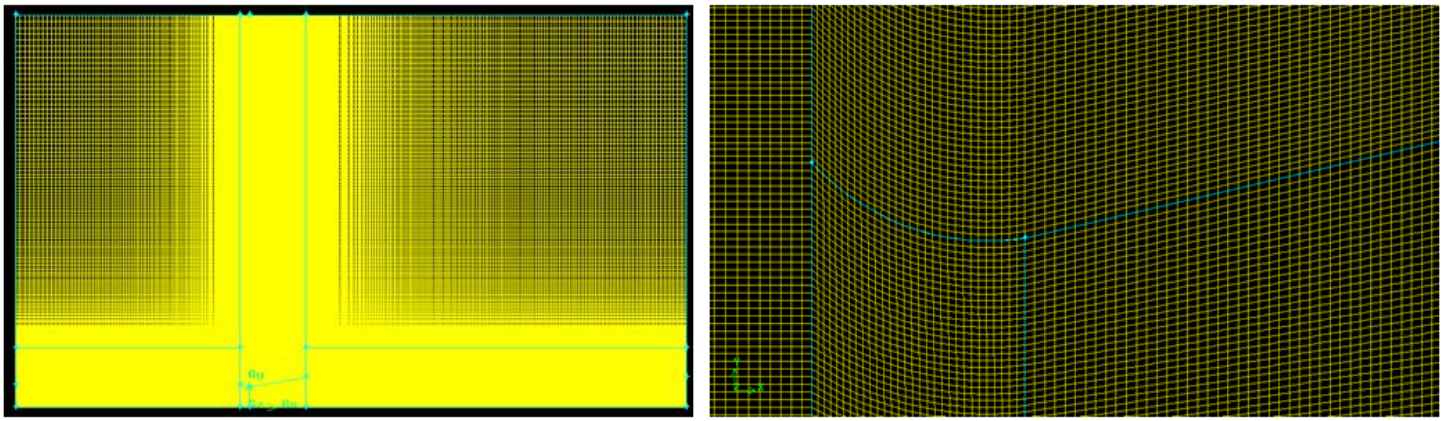

Fig. 2 Diffuser grid System with zooming mode

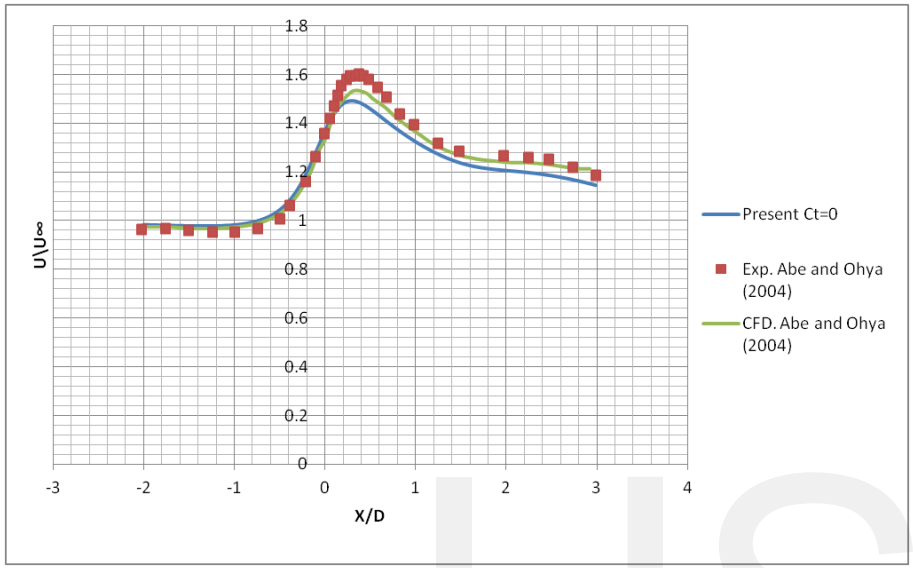

(a)

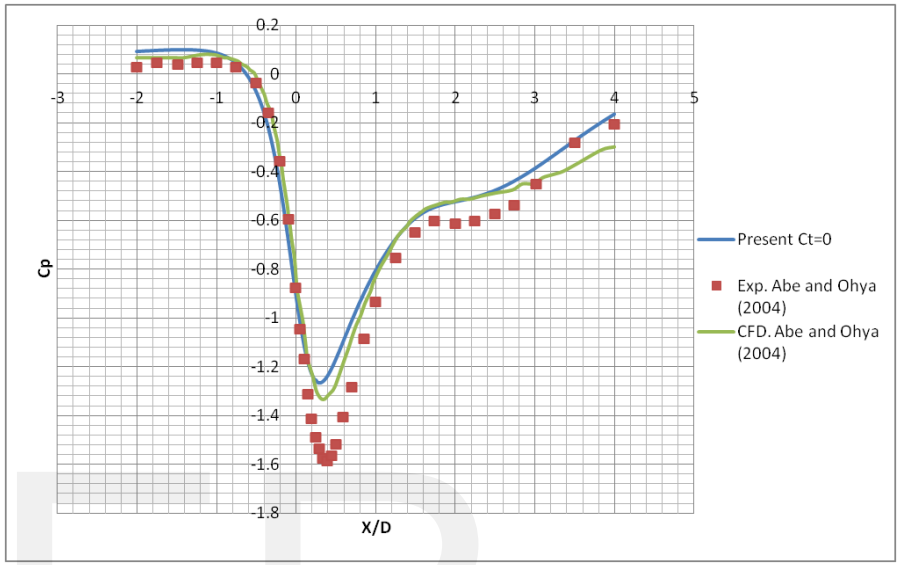

(b)

Fig. 3 Comparison of on-axis distributions of present work with Abe and Ohya (2004) Experimental and Numerical data at no load

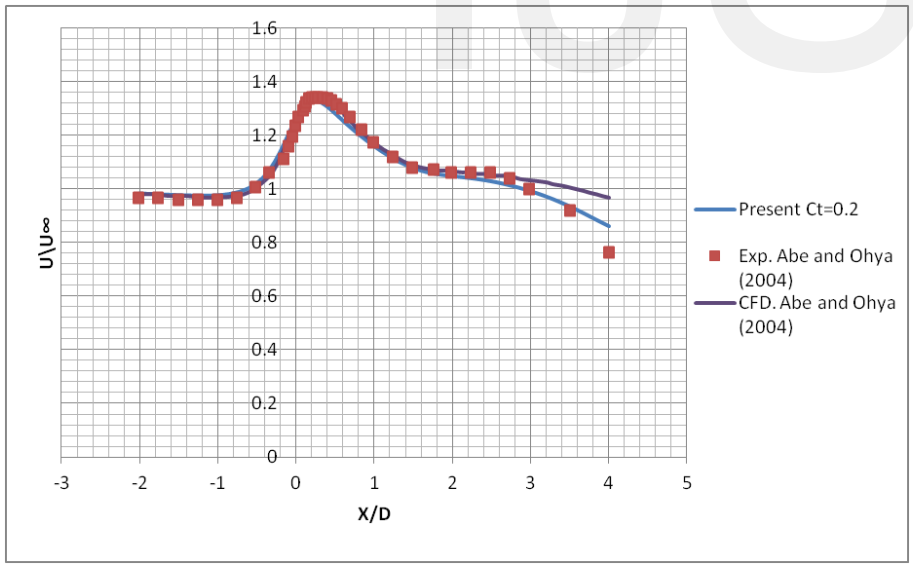

(a)

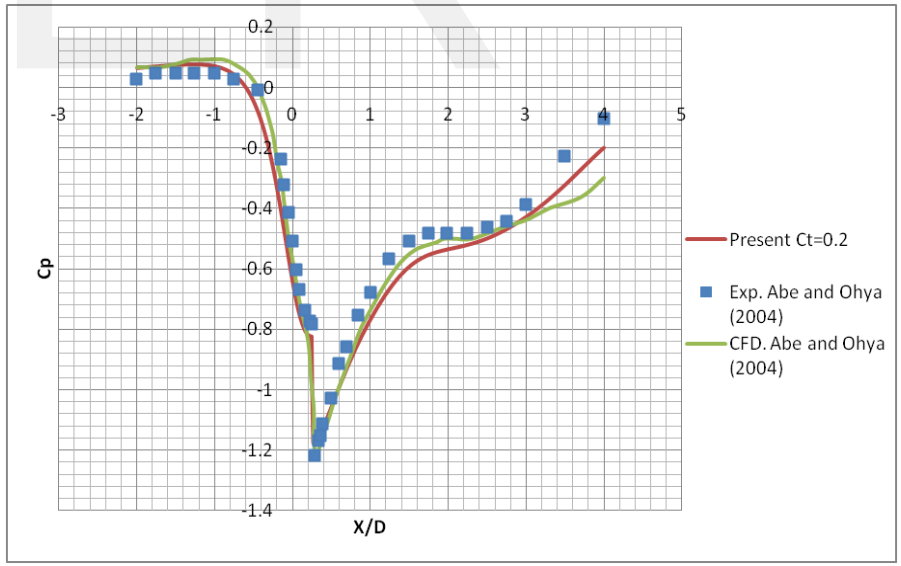

(b)

Fig. 4 Comparison of on-axis distributions of present work with Abe and Ohya (2004) Experimental and Numerical data at C_t=0.2

for velocity and pressure coefficient distribution respectively on the center axis, it is found that in generally good agreement with the corresponding experimental and numerical data, though a slight difference is seen. Also the results are in good agreement for C_t = 0.9 as shown in figure 5.a and 5.b. By comparing the effect of diffuser on the acceleration factor and input power shown in figure 6.a and 6.b respectively, it is show a good agreement with the corresponding experimental data.

4.2 Expansion angle effect

The main parameter affecting the flow passing though the diffuser is the inlet to outlet area ratio. At a fixed inlet diameter of the diffuser, the diffuser area ratio can be changed by changing either the diffuser expansion angle or the diffuser length. The effect of expansion angle on the velocity contours is presented in figure 7 for expansion angles of 0°, 2°, 4°, 6°, 8°, 10°, 12°, 14°, 16° and 18°. From this figure it is found that increasing the expansion angle leads to increase the velocity at the throat. That is due to the increasing in the outlet area, which increases the flow velocity inside the diffuser. So the fluid flow at the throat maintains its condition and accelerates through the diffuser throat. The results show that the flow pattern can be divided into two groups. The first group is the diffuser angles in the range of 0° and 12° as seen in figure 7.a to figure 7.g. For these values of the diffuser expansion angles, the air velocity at the throat increases as the expansion angle increases. This is due to increasing the outlet area of the diffuser. The second group is the case of higher degrees, more than 12°. For this case as seen in figure 7.h to figure 7.j, the velocity starts to decrease by increasing the expansion angle. This result is due to the recirculation occurred near the exit of the diffuser which decreases outlet flow area. The pressure contours are plotted at the same expansion angles as shown figure 8. From this figure it is found that increasing the diffuser expansion angle increases the external pressure acting on the diffuser outer body. It creates a high pressure region surrounding the diffuser, this region works as a resistance for the air flow that leads to force the air flow passing through the diffuser. Also increasing the expansion angle leads to decrease the pressure at the throat until the expansion angle reaches 12° as seen in figure 8.h. After this value of the expansion angle, the pressure starts to increase again as seen in figure 8.h to figure 8.j. The onset, development, and growth of steady lateral vortices or re-circulation in the diffuser with changing expansion angle are depicted in figure 9. Streamlines for flows with expansion angles of 0°, 2°, 4°, 6°, 8°, 10°, 12°, 14°, 16° and 18° are presented, where strong influences of expansion angle are evident. At low expansion angle, viscous forces dominate to produce undisturbed streamline flows and lateral vortex is damped. With increasing expansion angle (greater than 12°) secondary fluid circulation or swirl flow is generated near the end of the diffuser. The intensity and flow area coverage of this counter-rotating lateral vortex grows with expansion angle which leads to constant flow area while increasing the expansion angle. The axial wind velocity ratio ($U/U\infty$) and pressure coefficient distributions clearly reflect the influence of the expansion angle on the flow behavior as illustrated in figure 10, where the wind velocity ratio distribution along the diffuser center line are presented in figure 10.a for expansion angles having values of 0°, 2°, 4°, 6°, 8°, 10°, 12°, 14°, 16° and 18°. Likewise, in figure 10.b, the pressure coefficient distributions along the diffuser center line are presented at the same expansion angles (note: pressure coefficient is defined here as the ratio of the axial gage pressure over the dynamic pressure). The axial distribution of wind velocity ratio shows a high peak of wind velocity ratio at X/L = 0.2 starting from the diffuser inlet throat, as a result of the entrance chock at the diffuser inlet shroud due to flow attached to minimum cross section area values at the central axis. As the flow move toward the diffuser outlet, the wind velocity ratio decrease and the pressure coefficient increase as a result of increasing cross flow area. The increase in the expansion

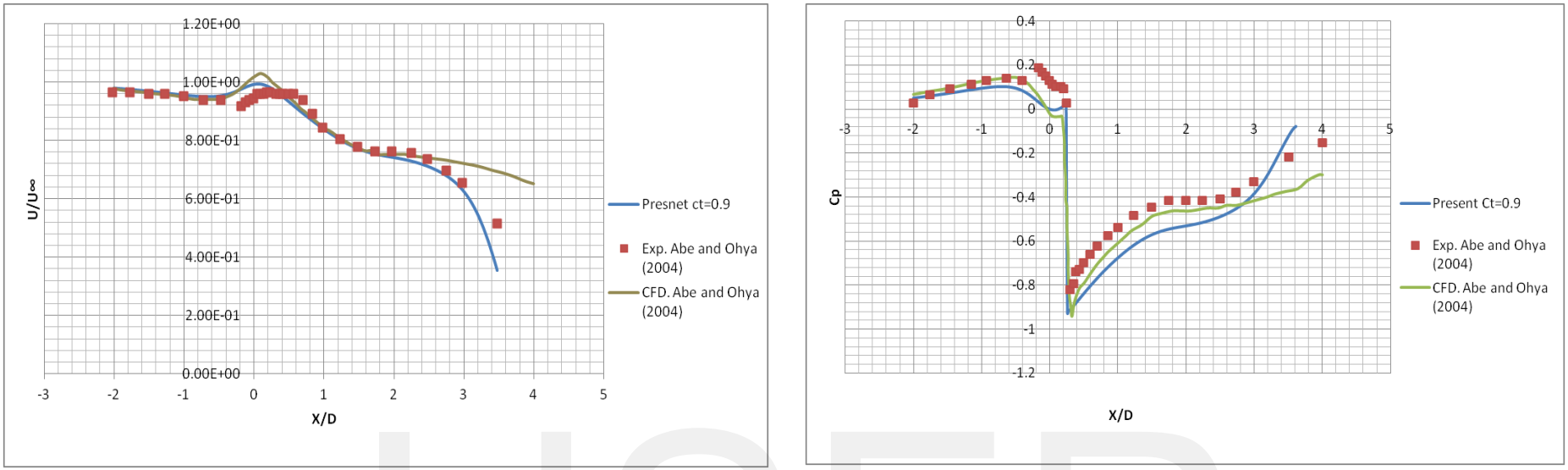

(a) (b)

Fig. 5 Comparison of on-axis distributions of present work with Abe and Ohya (2004) Expermental and CFD data at C_t=0.9

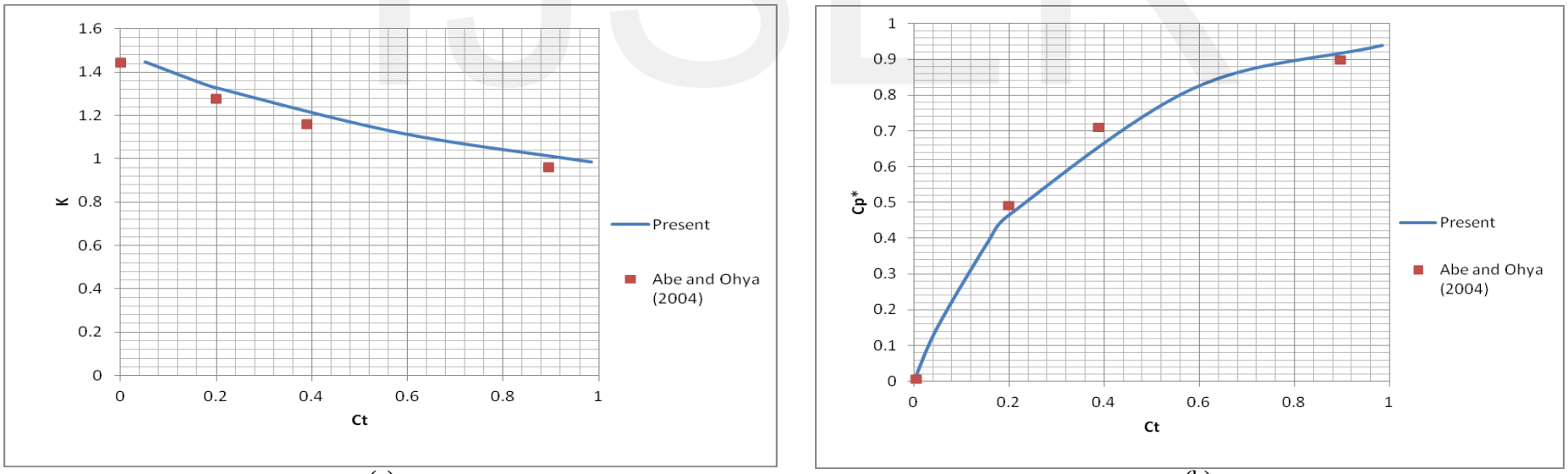

(a) (b)

Fig.6 Comparison between the effects of diffuser of present work with Abe and Ohya (2004) on performance:
(a) Acceleration factor; and (b) input-power coefficient

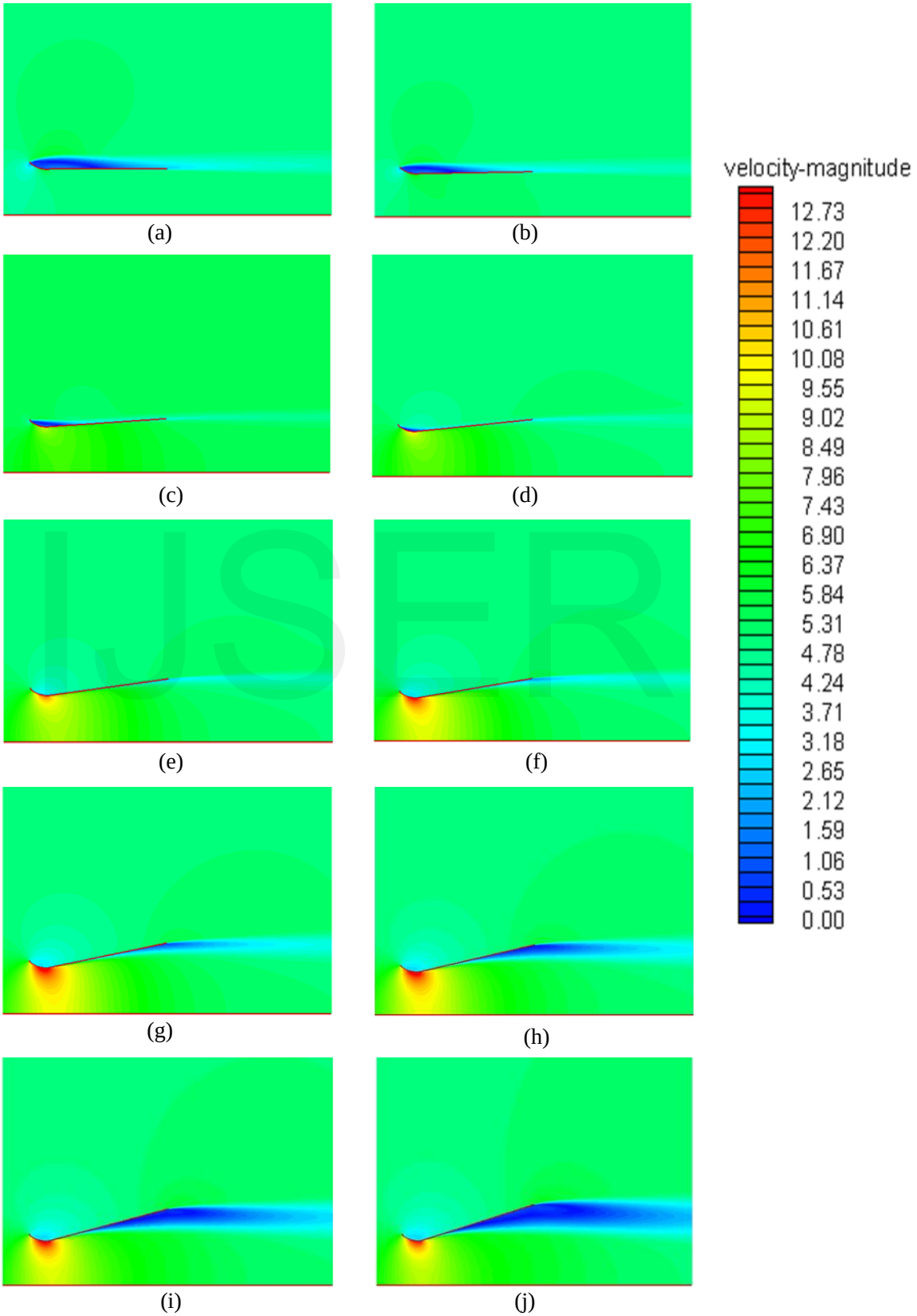

Fig.7 Velocity Contours in m/s at different diffuser expansion angles (a) 0°, (b) 2°, (c) 4°,(d) 6°,(e) 8°, (f) 10°,(g) 12°,(h) 14°,(i) 16° and (j) 18°.

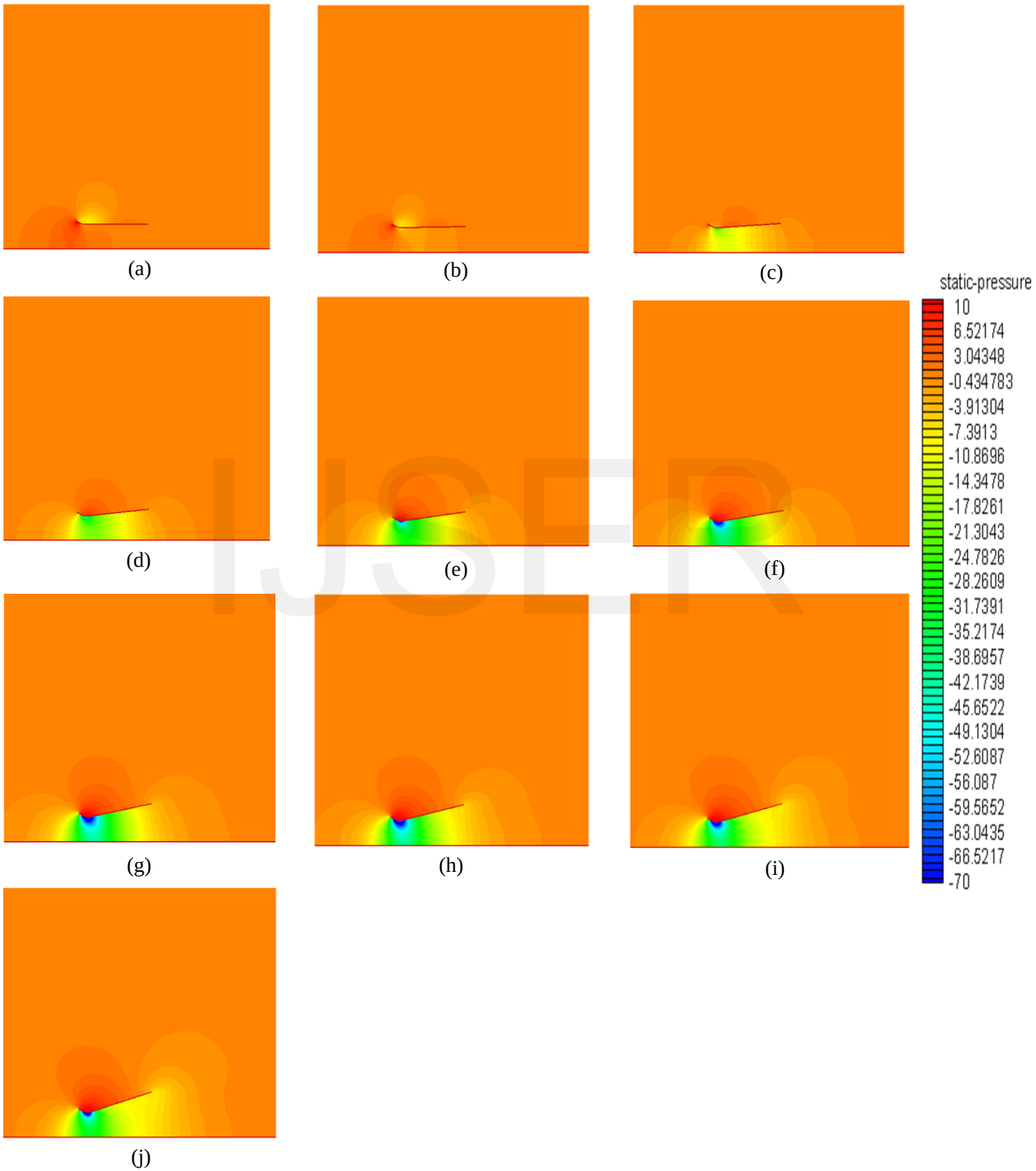

Fig. 8 Pressure Contours in Pascal at different diffuser expansion angles (a) 0°, (b) 2°, (c) 4°, (d) 6° (e) 8°, (f) 10°, (g) 12°,(h) 14°, (i) 16° and (j) 18°.

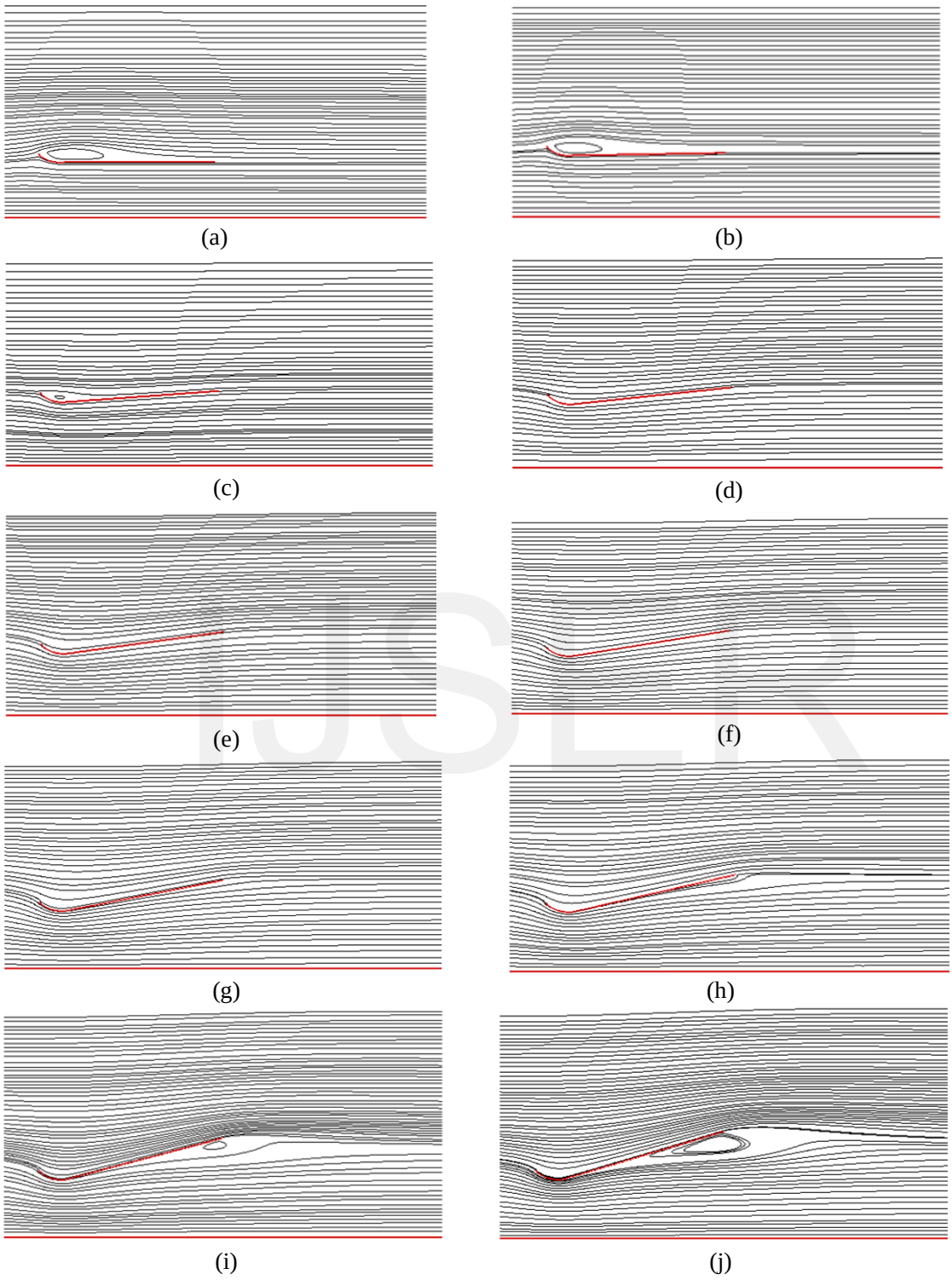

Fig. 9 a, b, c, d, e, f, g, h, i and j Stream lines at different diffuser expansion angles 0°, 2°, 4°, 6°, 8°, 10°, 12°, 14°, 16° and 18° respectively.

angle raised the wind velocity ratio and decreases the pressure coefficient at the throat. This is due the increasing in pressure at the end of the diffuser so the fluid flow will try to maintain its flow condition and accelerated through diffuser as mentioned before. As the expansion angle become larger than 12°, the wind velocity ratio starts to decreases. This is due to that the flow was unable to adopt the duct shape at angle higher than 12° as illustrated in figure 9. So flow recirculation occurs and the cross flow area remains constant along the diffuser in spite of increasing the expansion angle. The wind velocity ratio increased more steeply for angles less than 12° then it is started to decrease by increasing the expansion angle as illustrated figure 11.a where the wind velocity ratio is plotted against the expansion angle. Also in figure 11.b the linear decreasing in pressure coefficient at the diffuser outlet with increasing the expansion until reached to expansion angle 12°. Then it started to decrease.

4.2 Diffuser length effect

Figure 12 shows the effect of changing the diffuser length on the flow behavior inside and outside the diffuser. The velocity contours are presented for different diffuser lengths to inlet diameter ratio of 0.25, 0.5, 0.75, 1, 1.25, 1.5, 1.75 and 2 at diffuser expansion angle equal 12^o. It is clear from the figure that the velocity of the air flow at the throat increases with increasing the diffuser length due to increasing in the outlet area of the diffuser. So the fluid flow at the throat will try to maintain its flow condition and accelerated through diffuser. This phenomena is observed when the diffuser length to inlet diameter ratios is between 0.5 and 1.25. The other group is the case of longer diffuser, more than 1.25, where the separation occurred at the diffuser exit and increased as the diffuser length increase. This recirculation makes a nearly constant flow area so the change in velocity contour with diffuser length is small and can be negligible. The effect of diffuser length on the pressure contours is displayed in figure 13 at diffuser length to inlet diameter ratios having values of 0.25, 0.5, 0.75, 1, 1.25, 1.5, 1.75 and 2. It is observed that increasing the diffuser length causes to increase the external pressure acting on the outer diffuser wall and decreases the pressure at the diffuser throat which leads to increases the flow velocity inside the diffuser. These results are agreed with the velocity contours trend discussed previously in figure 12. By exceeding the diffuser length to inlet diameter ratio to 1.25 the change in pressure contours with length has little effects on the increasing the air velocity passing through the diffuser. Streamlines for flows inside and outside the diffuser with different length to inlet diameter ratios L/D of 0.5, 0.75, 1, 1.25, 1.5, 1.75 and 2 are presented in figure 14. The figure shows that when the diffuser length to inlet diameter ratio is between 0.5 and 1.25 the flow provides undisturbed streamline inside the diffuser. By increasing L/D more than 1.25 a separation formed at the end of the diffuser and it increases with increasing diffuser length which leads to a constant cross flow area whatever increasing the diffuser length. Figure 15.a shows the wind velocity distribution $U/U\infty$ on the central axis of the diffuser at length to inlet diameter ratios (L/D) of 0.25, 0.75, 1, 1.25, 1.5, 1.75 and 2. Hence X/L = 0 is the model entrance and X/L = 0.21, 0.34, 0.45, 0.56, 0.67, 0.78, 0.89 and 1 is the model exit at diffuser body 0.25, 0.5, 0.75, 1, 1.25, 1.5, 1.75 and 2 respectively. From the figure it is found that the longer the main body, the higher the air velocity. Also the maximum wind speed is obtained at the diffuser throat. The increasing in the L/D initially raised the wind speed ratio until L/D=1.25, but when L/D become larger, the rate of increasing in velocity with diffuser length is decreased due to the separation formation as discussed before. The axial pressure coefficient distribution for the same values of the different diffuser length to inlet diameter ratio is plotted in figure 15.b. From this figure it is found that the pressure at the diffuser throat decreases by increasing the diffuser length, which reflects increasing in the velocity passing through

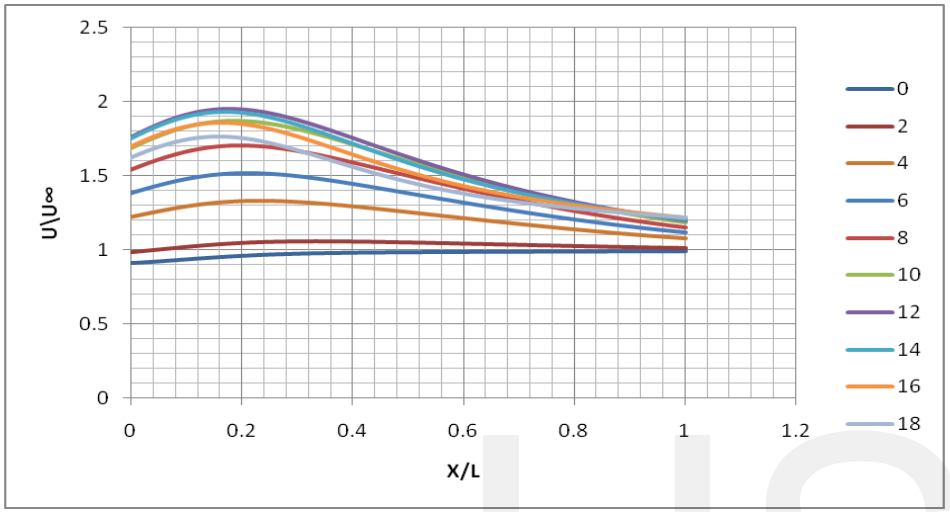

(a)

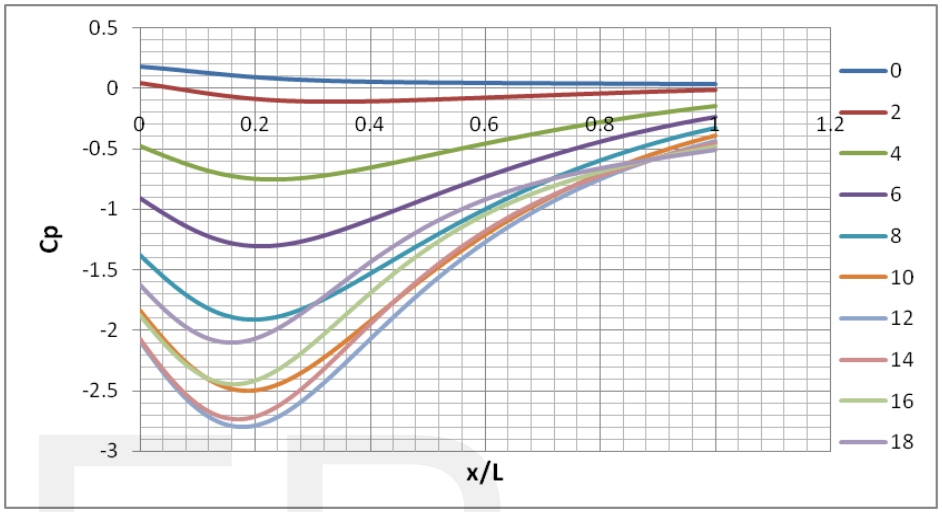

(b)

Fig. 10 Wind velocity ratio and static pressure distributions on the central axis at different angles 0°, 2°, 4°, 6°, 8°, 10°, 12°, 14°, 16° and 18° (a) wind velocity and (b) static pressure coefficient.

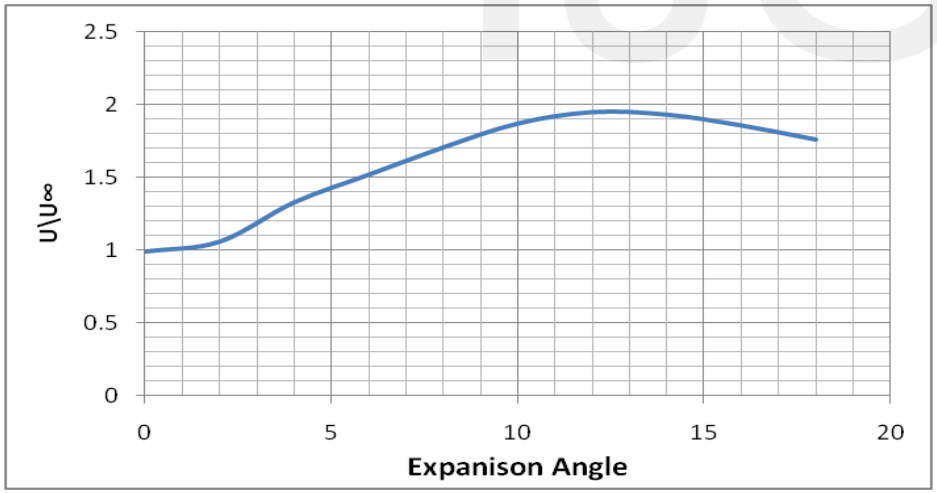

(a)

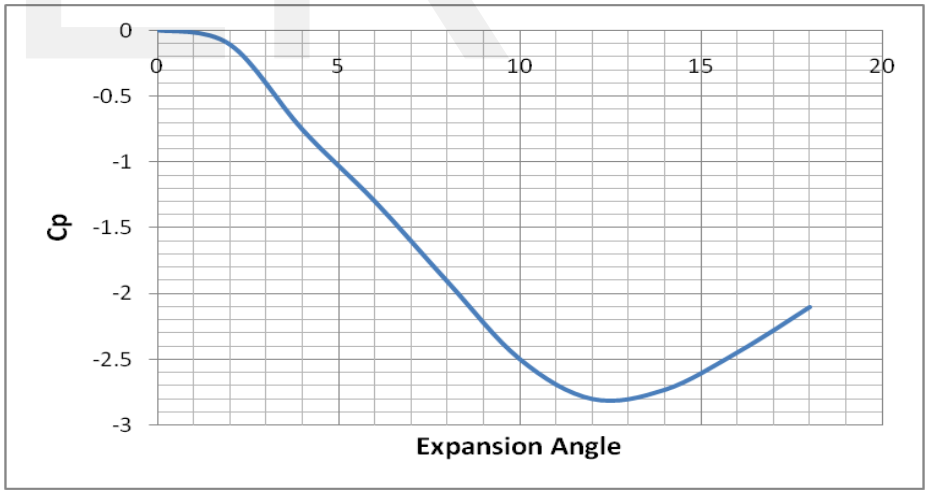

(b)

Fig. 11 (a) Velocity magnitude and (b) Outlet Static pressure coefficient at central axis at many different diffuser expansion angles.

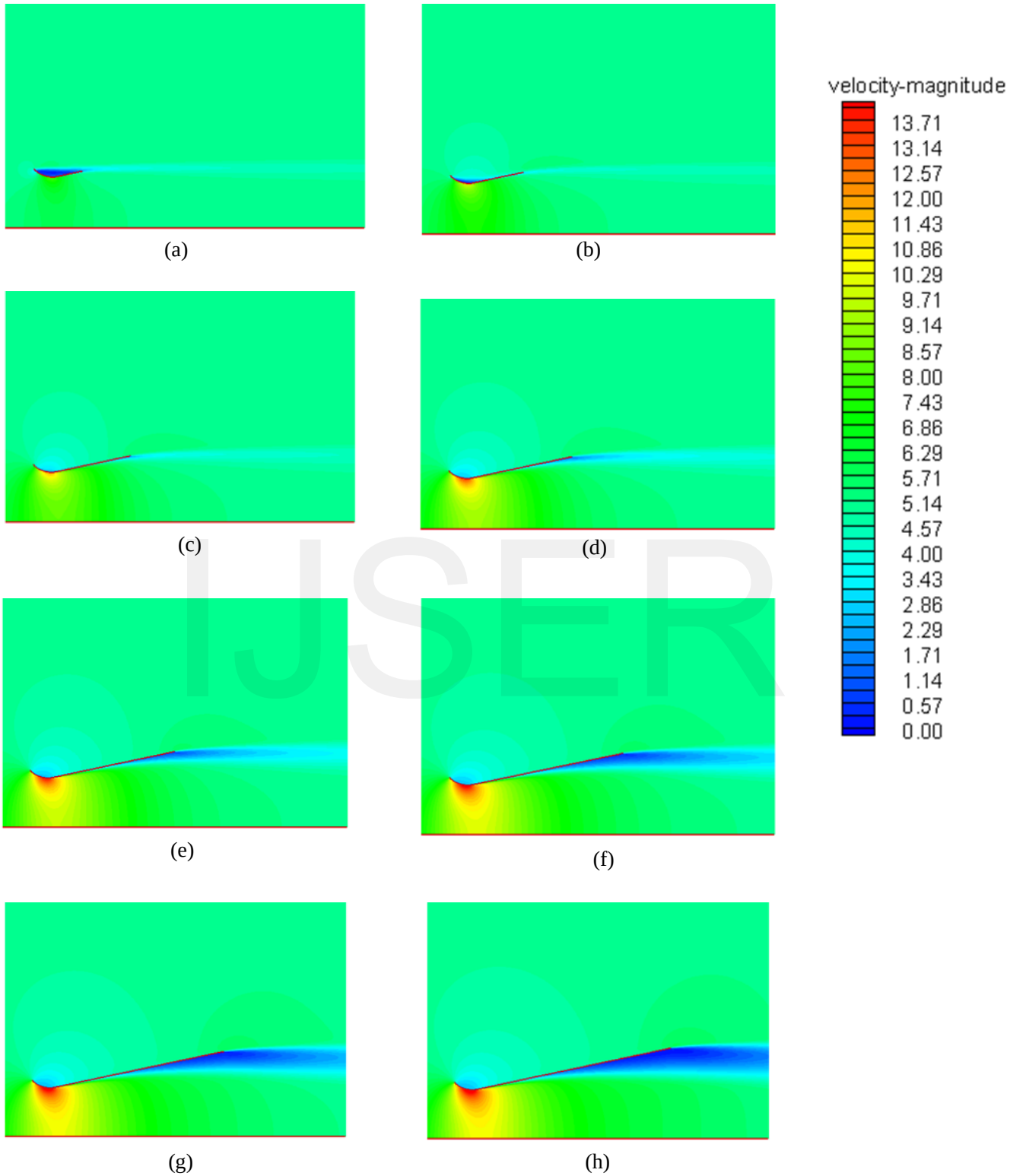

Fig. 12 (a, b, c, d, e, f, g and h) Velocity magnitude contours in m/s at different diffuser length to inlet diameter ratio 0.25, 0.5, 0.75, 1, 1.25, 1.5, 1.75 and 2, respectively.

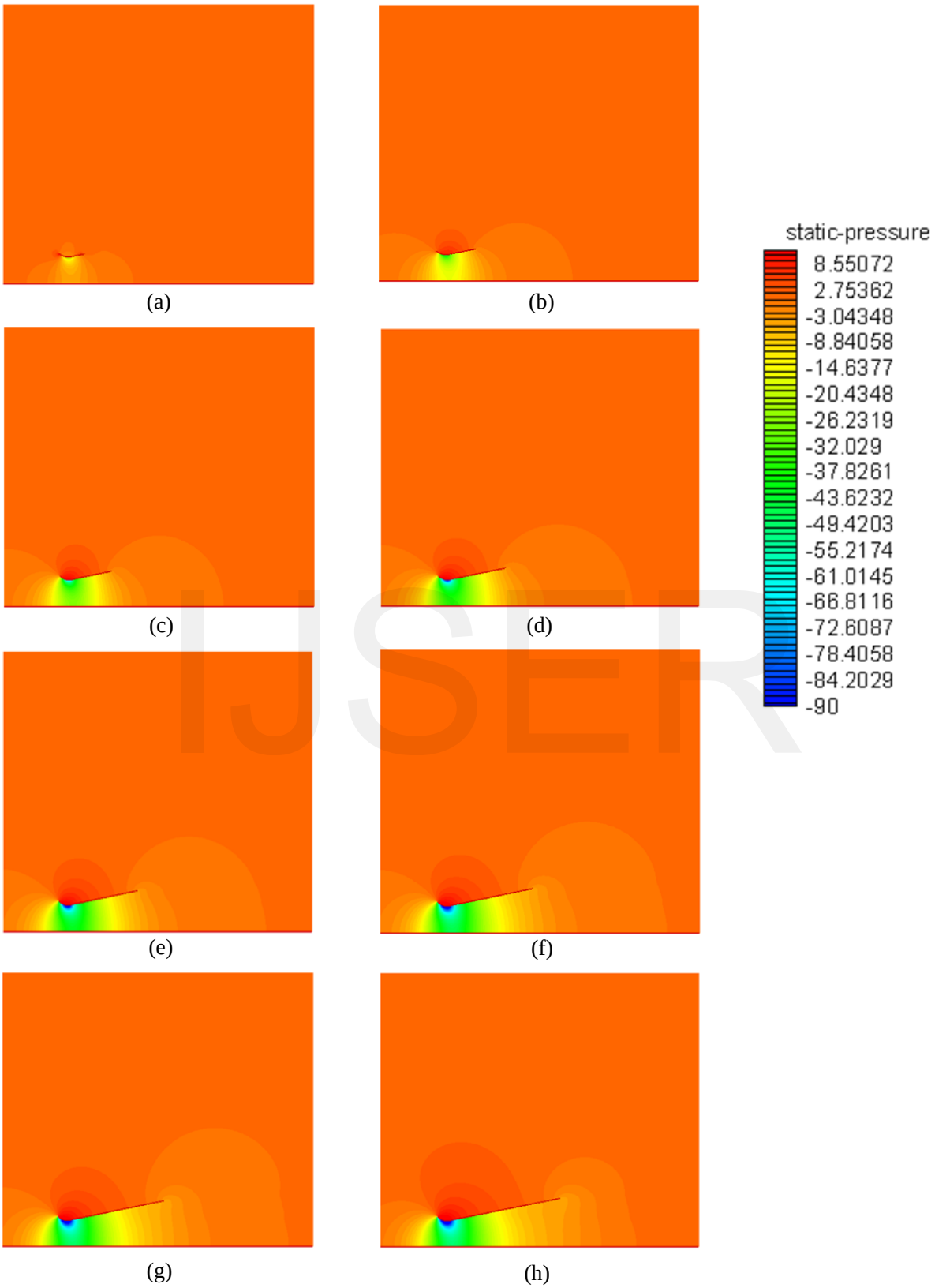

Fig.13 (a, b, c, d, e, f, g and h) Static Pressure contours in Pascal at different diffuser length to inlet diameter ratio L/D 0.25, 0.5, 0.75, 1, 1.25, 1.5, 1.75 and 2 respectively

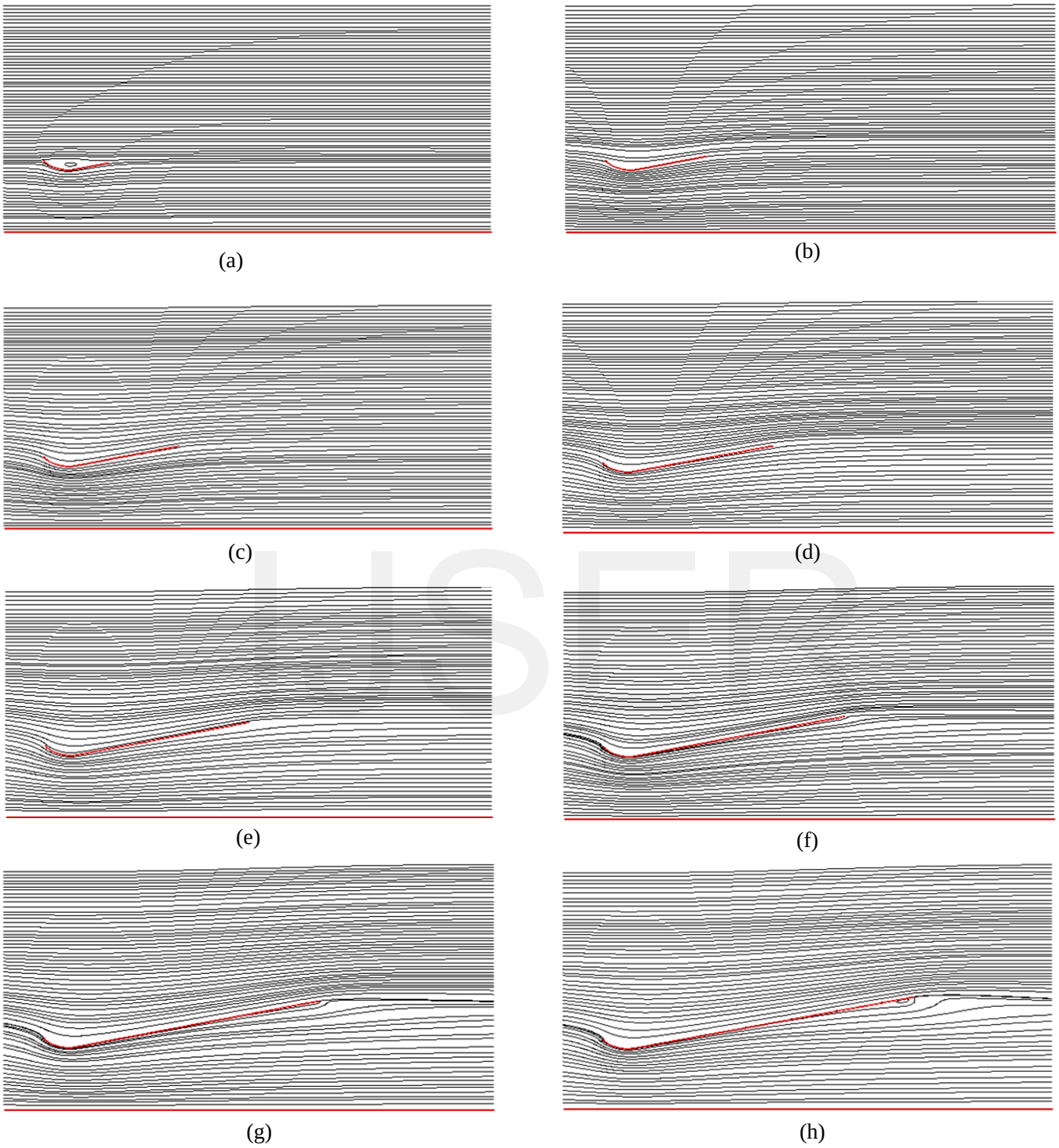

Fig. 14 (a, b, c, d, e, f, g and h) shows stream function at different diffuser length to inlet diameter ratio 0.25, 0.5, 0.75, 1, 1.25, 1.5, 1.75 and 2 respectively.

the diffuser but as discussed before a separation formed at the exit of the diffuser after exceeding the diffuser length to inlet diameter ratio the value of 1.25 which decreases by its turn the velocity passing through the diffuser. From figure 16.a it is concluded that the maximum velocity at the central axis of the diffuser increases with increasing the diffuser length to inlet diameter ratio until reached to 1.25. By exceeding this value, the rate of increasing in the velocity starts to decrease. By plotting the static pressure coefficient at diffuser throat on central axis as shown in figure 16.b, it is found that the pressure coefficient decreases steeply until reaches to L/D = 1.25 then the rate of decreasing in the pressure coefficient at diffuser throat starts to decrease. In practice it is desirable to have diffuser with L/D as small as possible to limit the cost so the diffuser length to diameter ratio having a value of 1.25 is considered as an optimum value for cost limitation and to prevent a recirculation occurred at the end of diffuser when L/D ratio becomes larger than 1.25 . By plotting the maximum wind velocity on the central axis of a diffuser type at different length to inlet diameter ratio at many expansion angles as shown in figure 17, It is found that when the diffuser outlet area to inlet area ratio increases due to the increasing in the diffuser length or the expansion angle, the flow velocity passing through the diffuser throat increases. But when the diffuser outlet to inlet area ratio exceeds a certain value, a flow separation formed at the end of the diffuser which decreases the outlet area and the velocity passing through the diffuser.

4.3 Flange height effect

Focusing on the pressure contours as shown in figure. 18 for different flange height to inlet diameter ratio (h/D) having values 0, 0.375, 0.5, 0.625, 0.75, 0.875 and 1. It is found that a high pressure region is formed in front of the flange and increase with increasing flange height. This high pressure region makes higher flow resistance outside the diffuser which leads to increase the overall flow speed inside the diffuser with increasing flange height. The flange also generates a low pressure region behind it which increases by increasing the flange height. This creates a suction region which affects also in increasing the velocity inside the diffuser with increasing the flange height. From these analyses, it is found that the flange is playing a significant role in local pressure drop which ultimately results in drawing more wind at the inlet throat. Figure 19 shows velocity contours for different flange height to inlet diameter ratio (h/D) with values of 0, 0.375, 0.5, 0.625, 0.75, 0.875 and 1. It shows that the greater the flange height, the higher the wind speed at the throat, till flange height to diffuser diameter ratio (h/D) equal 0.75, after that the rate of increasing of velocity with flange height is decreased and can be negligible. In the form of the streamlines plots. There is a significant recirculation region in the diffuser equipped with a flange than is not present in the diffuser without a flange case as shown in figure 20 which present an overall view of the flow field around the flanged diffuser at different flange height to inlet diameter ratio 0, 0.375, 0.5, 0.625, 0.75, 0.875 and 1. As seen in the figure, a flange generates a large separation behind it. This is a notable feature of this kind of flow field; this separation generates a low-pressure region in the near wake of the diffuser owing to the vortex formation and draws the flow into the diffuser. The vortex formation like the von Karman vortex street is seen downstream of the flange. Also it is clearly observed from this figure that as higher the flange height as higher the vortices region behind the diffuser. As mentioned before by increasing this region a low pressure region will increase at the downstream of the diffuser which make increase in velocity inside the diffuser. Figures. 21.a, b show the wind velocity ratio distribution U/U_∞ and static pressure coefficient distribution Cp on the central axis of a diffuser equipped with flange at different flange height to inlet diameter ratio 0, 0.375, 0.5, 0.625, 0.75, 0.875 and 1. As seen in figure. 21.a, b the flanged diffuser model has a remarkable effect on the collection and

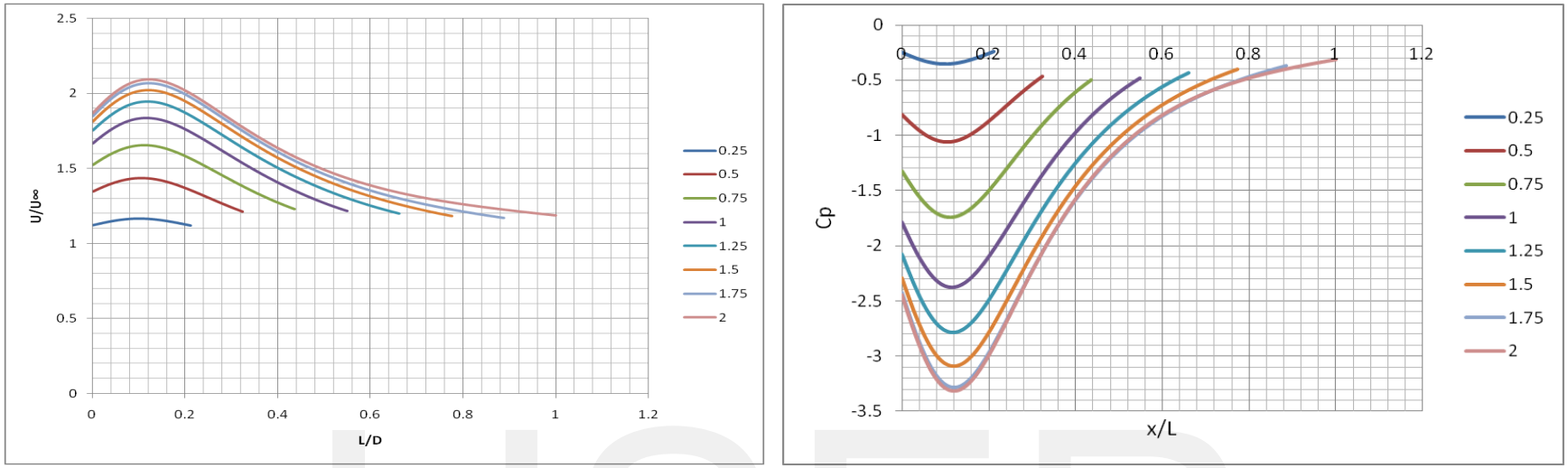

(a) (b)

Fig. 15 Wind velocity and static pressure distributions on the central axis of a diffuser type at different length inlet diameter ratio are 0.25, 0.5, 0.75, 1, 1.25, 1.5, 1.75 and 2 (a) wind velocity and (b) static pressure distribution.

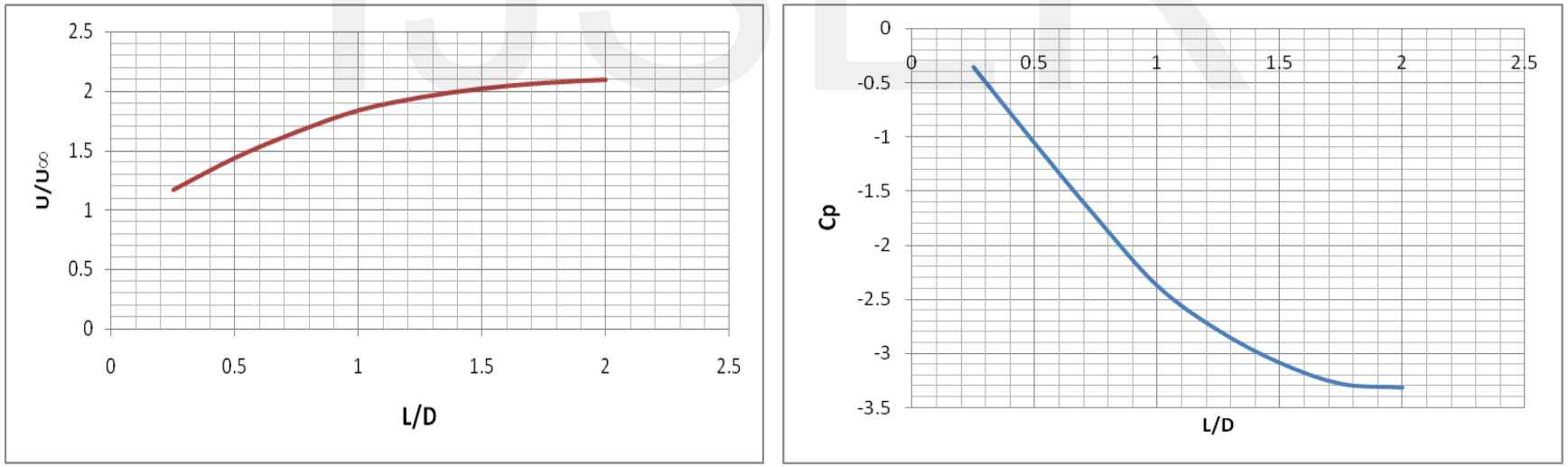

(a) (b)

Fig. 16 (a) Velocity magnitude and (b) Outlet Static pressure coefficient at central axis at many different diffuser expansion angles.

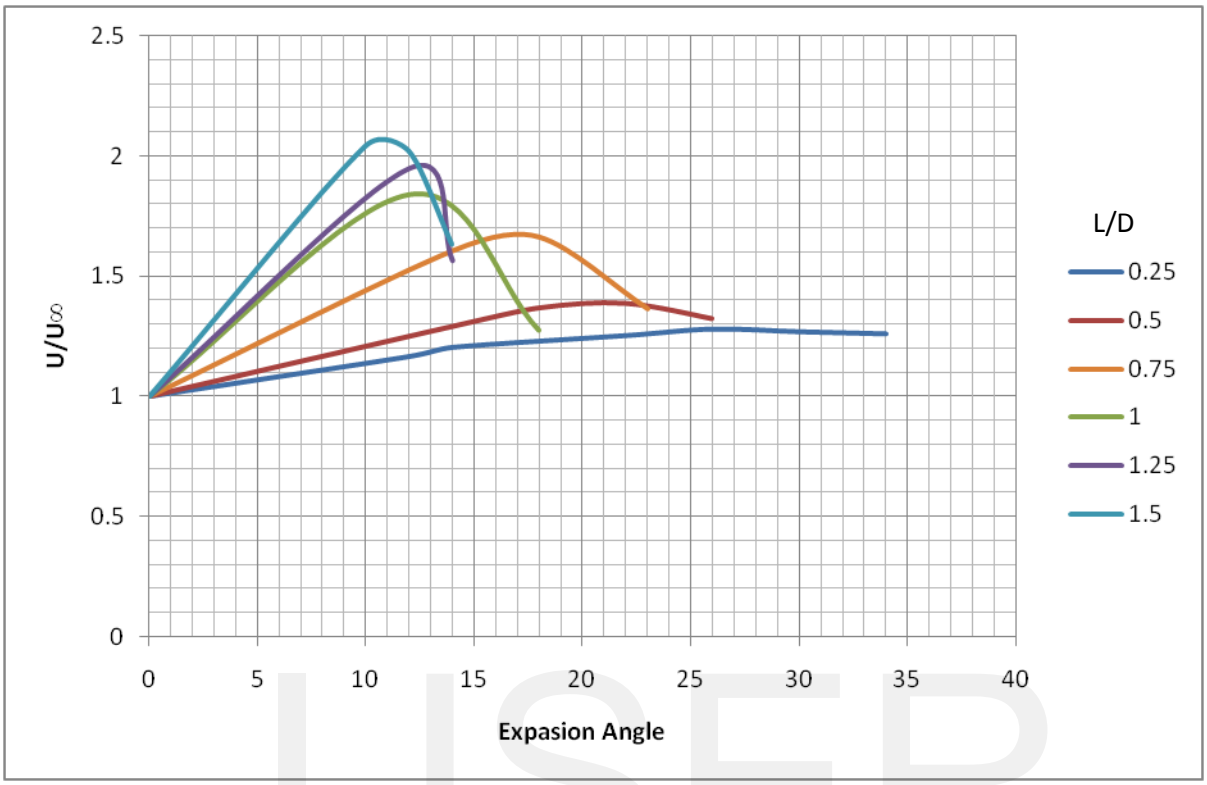

Fig. 17 Maximum wind velocity on the central axis of a diffuser at different length to inlet diameter ratio at many expansion angles.

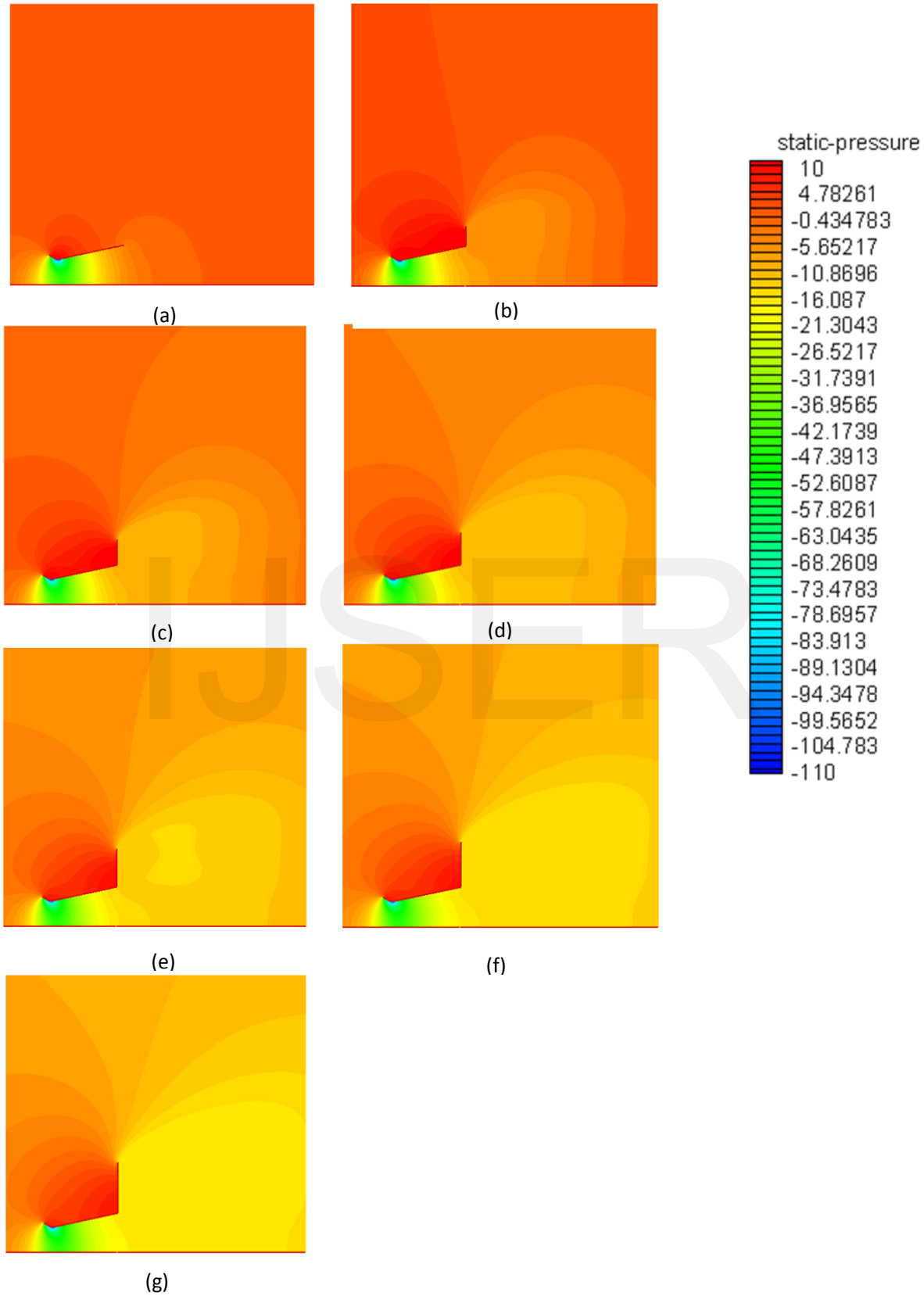

Fig.18 Pressure Contours in Pascal at different flange height to inlet diameter ratio (a) 0, (b) 0.375, (c) 0.5, (d) 0.625, (e) 0.75, (f) 0.875 and (g) 1.

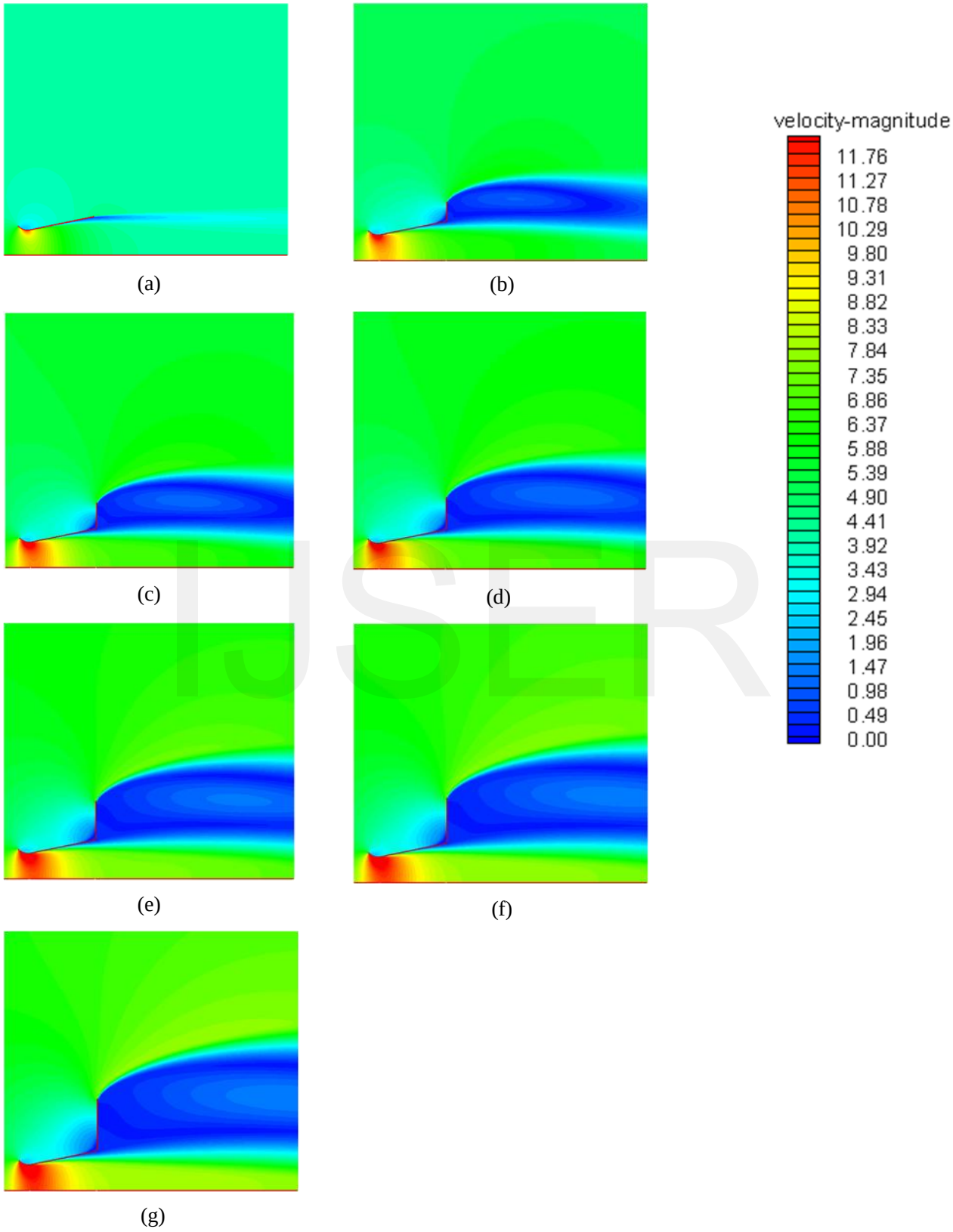

Fig.19 Velocity Contours of the air flow in m/s at different flange height to inlet diameter ratio (a) 0, (b) 0.375, (c) 0.5, (d) 0.625, (e) 0.75, (f) 0.875 and (g) 1.

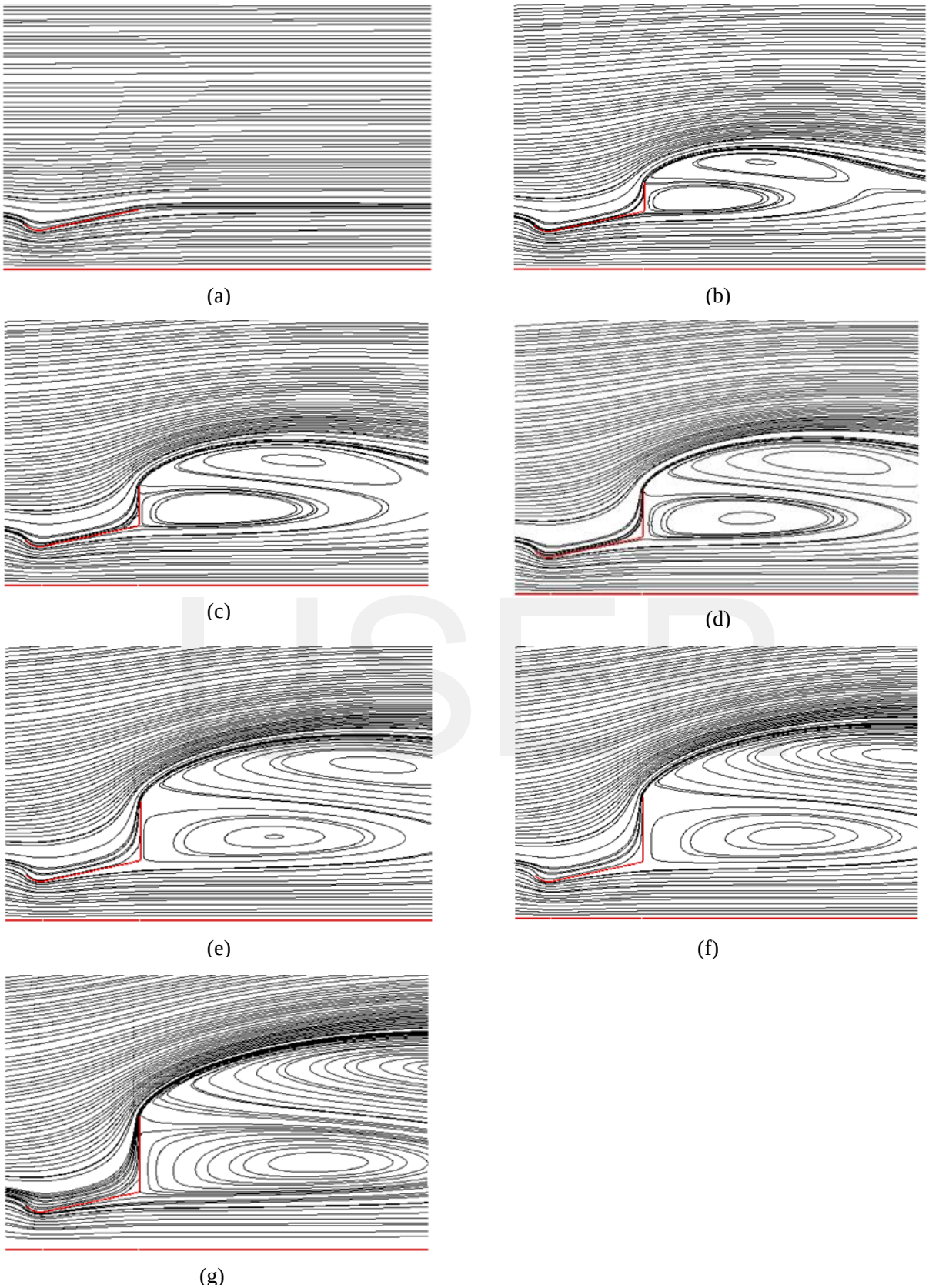

Fig.20 Streamlines at different flange height to inlet diameter ratio
(a) 0, (b) 0.375, (c) 0.5, (d) 0.625, (e) 0.75, (f) 0.875 and (g) 1.

acceleration of the approaching wind and the greater flange height, the higher the wind speeds at the throat (Maximum velocity ratio at the centerline) and lower pressure coefficient at the throat of the diffuser, till flange height to diffuser diameter ratio reaches to 0.75. After this value, the rate of change of velocity with flange height is relatively small so flange height to diffuser diameter ratio 0.75 is the best value for diffuser design. Figure 22.a shows the summary of changing the maximum velocity at the diffuser center line with different flange height to inlet diameter ratio. The velocity increases by increasing h/D to 0.75. Then the rate of change starts to decrease. Also by focusing on the figure 22.b it is concluded that the diffuser outlet pressure coefficient decreases by using a flange.

4.4 Load factor effect

To determine the performance of the diffuser having a wind turbine inside, it is possible to replace the turbine rotor by just a load factor because both of the wind turbine rotor and the load factor have a common concept of creating a pressure drop in their downstream. Figure 23 a, b, c, d, e, f, g and h represents the static Pressure contours at different load factor C_t equal to 0, 0.156, 0.274, 0.432, 0.551, 0.668, 0.826, and 0.944, respectively. It demonstrates the pressure contours for the case when the rotor is replaced by just a load factor. Comparing figure 23.a which represents the empty diffuser (no load) with figure 23.b which represents a load factor equal to 0.156, it can be seen that the pressure drop in the load area is quite tangible due to the presence of this volume force. By increasing the load factor the pressure drop increases at the position of the turbine rotor as seen in figure 23 c, d, e, f, g and h. In deed the load factor also has a negative effect on the air velocity passing through the diffuser as the actual wind turbine does. By comparing the velocity contours of the empty diffuser as represented in figure 24.a and figure 24.b which represents a load factor equal 0.156, it is found that the velocity decreases at the throat in case of adding a load factor and continue in decreasing by increasing the load factor, as seen in figure 24 c, d, e, f, g and h. Pressure coefficient distribution and wind relative velocity ratio on the central axis of the diffuser are plotted in figure 25.a and 25.b respectively at load factors 0, 0.156, 0.274, 0.432, 0.551, 0.668, 0.826, and 0.944. The discontinuity in the pressure profile reflects the load as shown in figure 25.a, while the velocity varies continuously due to the restriction of the continuity equation as shown in figure 25.b. It is seen from the figure that the present computation returns generally reasonable trends for the variation of the loading coefficient, though its accuracy is not perfect. As the loading coefficient increases, the maximum velocity decreases and the discontinuity in the pressure profile becomes larger. It is interesting that even the case of C_t = 0.95 still provides a high level of the maximum velocity ratio around 1.05, which can never be achieved by a bare wind turbine. Figure 26 a, b, c and d shows the effect of the load of the designed flanged diffuser on acceleration factor, input-power coefficient, base pressure coefficient and pressure recovery coefficient respectively. By plotting the relation between the acceleration factor K and the load factor C_t in figure 26.a (Noted that the acceleration factor is defined as the ratio between the load inlet air velocity to the free stream velocity), it is found that by increasing the load factor the acceleration factor decreases until reached to value of C_t equal 0.95, at this value of the load factor the acceleration factor is still > 1. In another word the designed diffuser is still effective and able to increase the air velocity passing through it. By increasing C_t more than 0.95 the diffuser will not be effective in increasing the velocity and the acceleration factor will be lower than 1. Figure 26.b which represent the relation between the load factor and the input power Cp* (Cp* is defined as the load factor multiplied to the cubic acceleration factor), from this figure it is concluded that in the range of C_t lower than 0.4, the diffuser performance is not so high, thus t he bes t C_t is

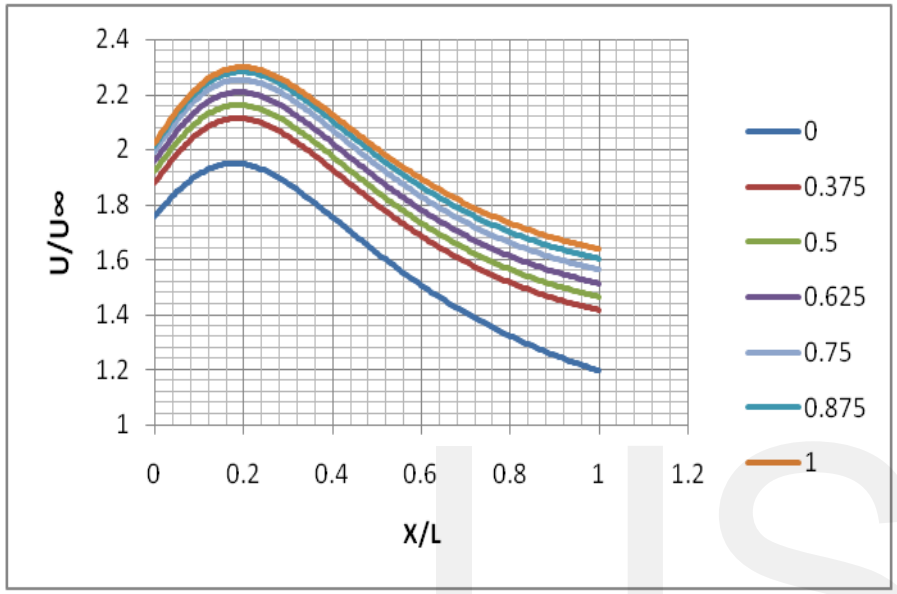

(a)

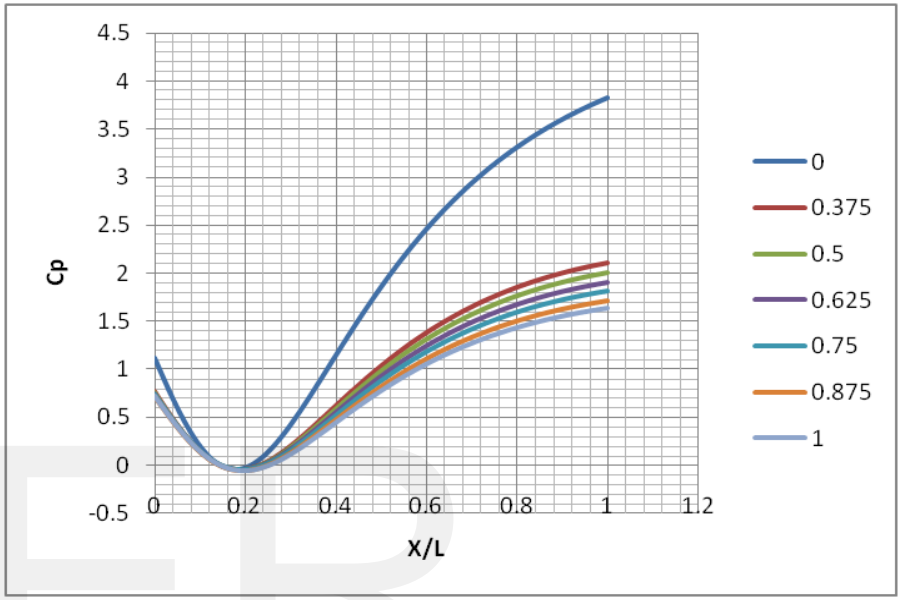

(b)

Fig.21. Wind velocity ratio and static pressure coefficient distributions on the central axis of a diffuser at different flange height to inlet diameter ratio (a) wind velocity ratio and (b) static pressure coefficient.

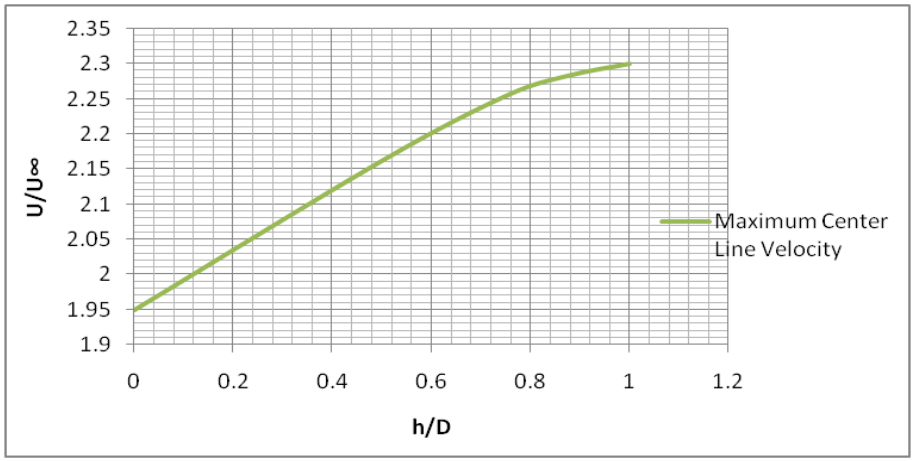

(a)

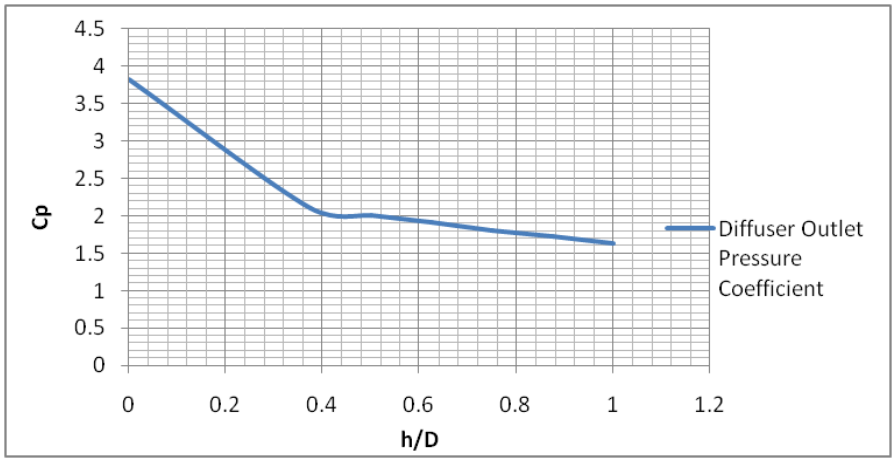

(b)

Fig.22 (a) Maximum Center line velocity (b) Outlet Static pressure coefficient at central axis.

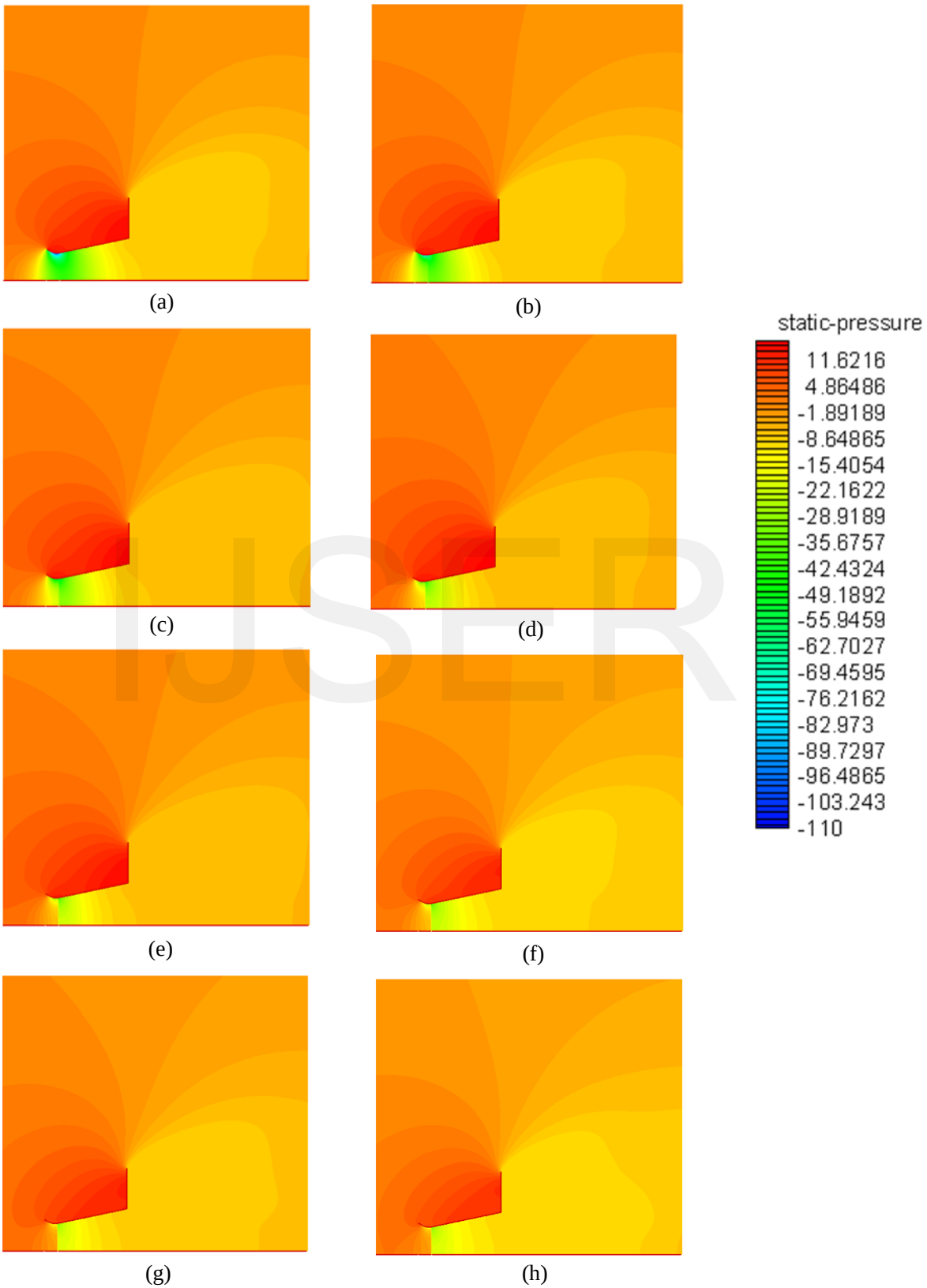

Fig 23 a, b, c, d, e, f, g and h. Static Pressure contours in Pascal at different load factor C_t= 0, 0.156, 0.274, 0.432, 0.551, 0.668, 0.826, and 0.944, respectively

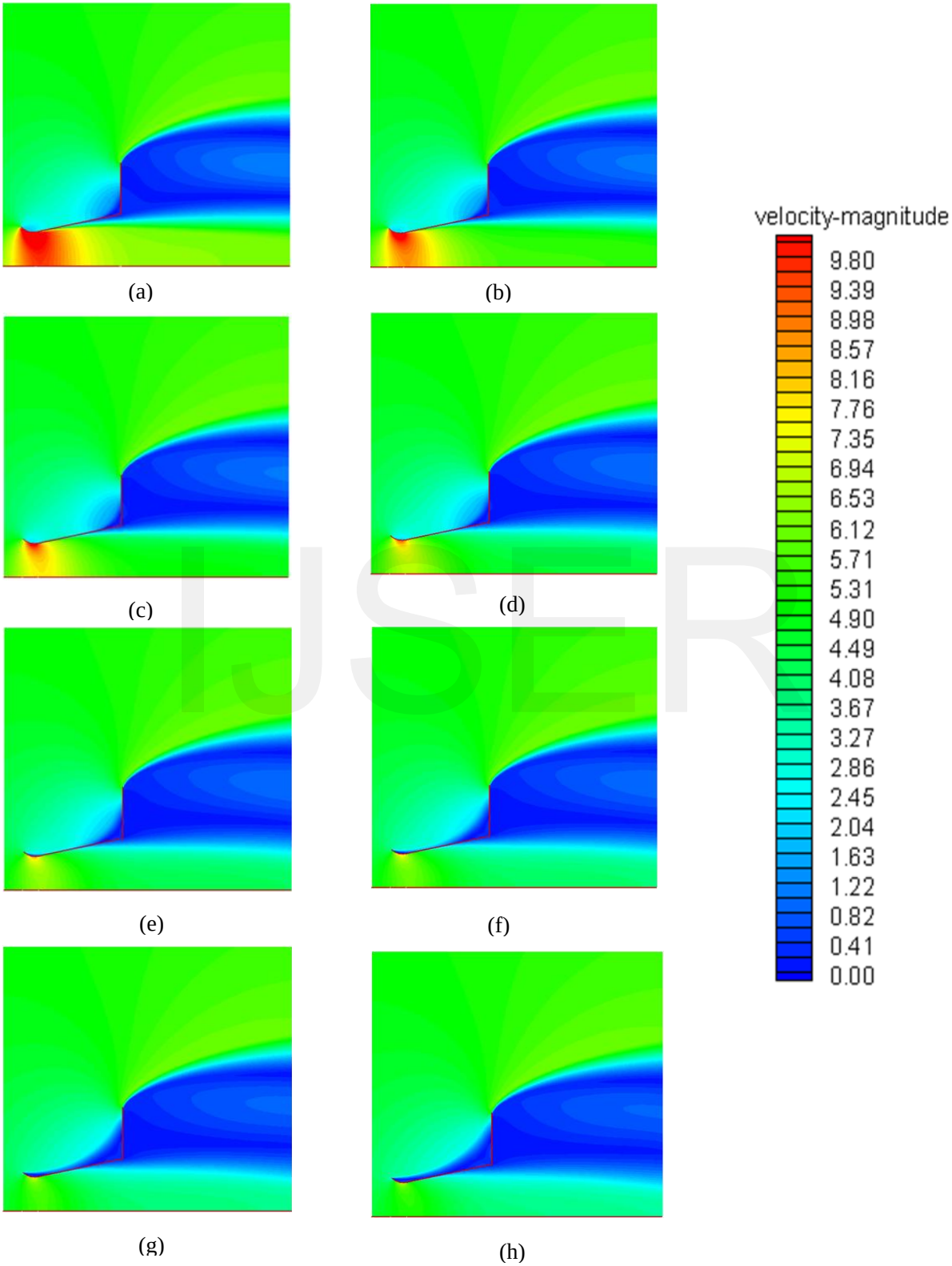

Fig 24 a, b, c, d, e, f, g and h. Velocity contours in m/s at different load factor C_t= 0, 0.156, 0.274, 0.432, 0.551, 0.668, 0.826, and 0.944 respectively

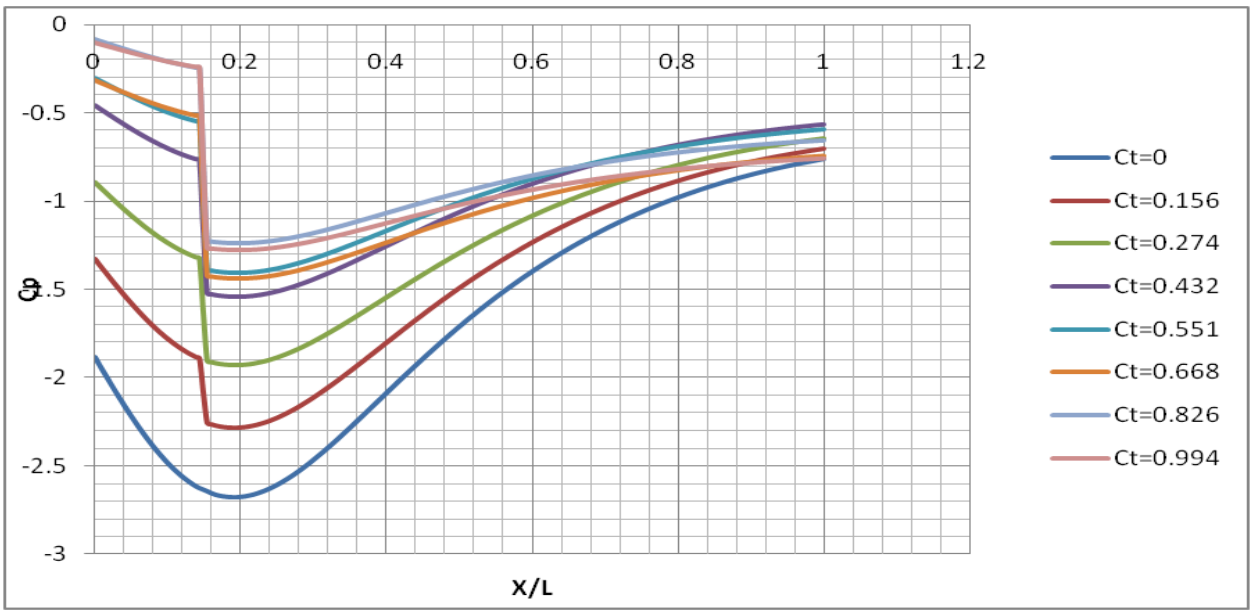

(a)

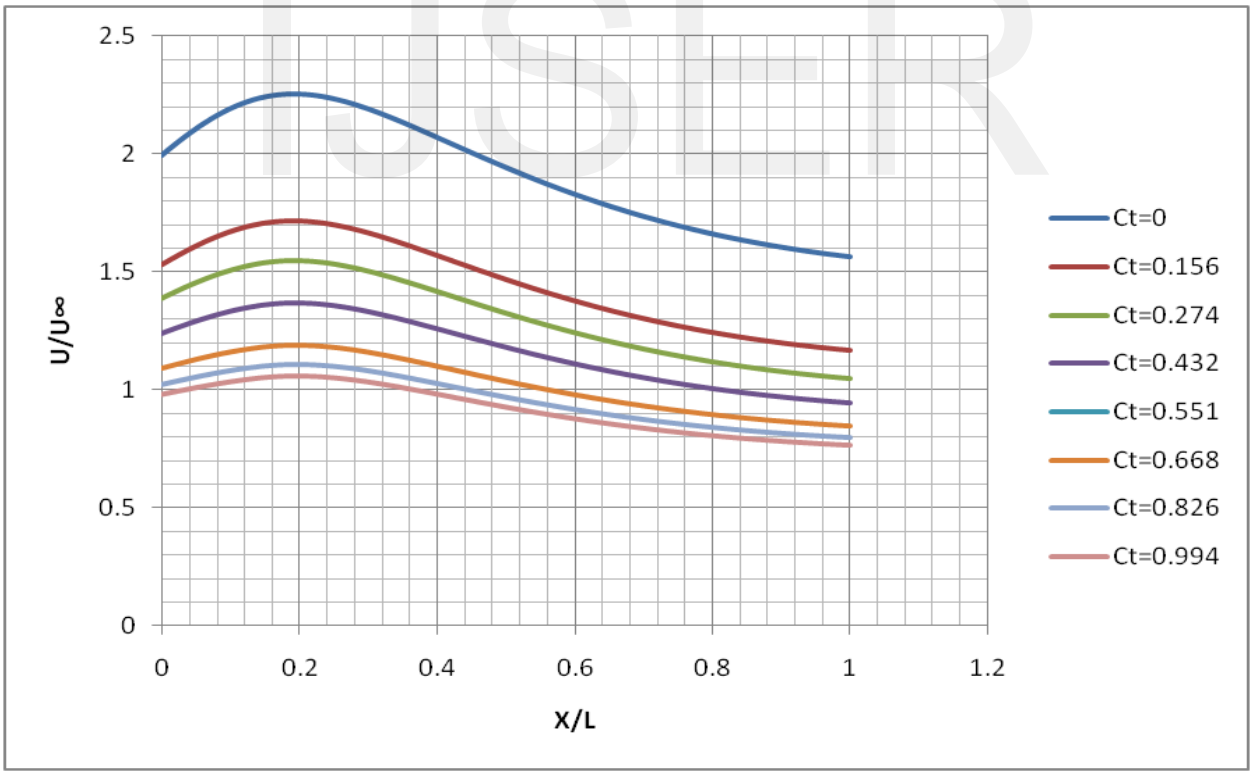

(b)

Fig.25 Comparison of on-axis distributions L/D=1.25, Φ=12^{o}, h/D=0.25, at different load factor : (a) pressure coefficient and (b) streamwise velocity

estimated to be 0.4 to 0.95, also from this figure it is confirmed that the highest performance is actually achieved at C_t ranged from 0.4 to 0.95. The base pressure coefficient Cp_b which is defined as the ratio of the difference of the pressure at the outlet of the diffuser and the ambient pressure to the dynamic pressure of the free stream is plotted against the load coefficient in figure 26.c. From this figure it is found that increasing the load factor, increase the base pressure coefficient until the value of C_t equal to 0.95, by exceeding C_t more than this value, the base pressure coefficient approach to 0, this mean that the pressure at the exit of the diffuser is equal to the ambient pressure which eliminate the main function of the diffuser of increasing the pressure at the exit of the diffuser, by its turn it leads to make the diffuser has no role in increasing the velocity passing through it. At this case the diffuser shape effects turned to a cylindrical shape effects. By graphing the pressure recovery coefficient Cp_d (which is defined as the ratio of the difference between the pressure at exit of the load and the pressure at the exit of the diffuser to the dynamic pressure of the free stream) versus the load coefficient, it is found that when the load factor increases it causes to increase the pressure recovery coefficient as shown in figure 26.d. It is important to mention that figure 26 can be used as a design guide for the required wind turbine to place it in the designed diffuser to get an optimum output power.

4 Conclusion

1. Increasing the expansion angle leads to increase the velocity of the air flow at the throat and decrease the static pressure when the diffuser angles are between 0° and 12° after that the velocity and pressure remains a fixed value whatever increasing in expansion angle due to recirculation effect.
2. At low expansion angle, viscous forces dominate to produce undisturbed streamline flows and lateral vortex is damped. With increasing expansion angle (greater than 12°.) secondary fluid circulation or swirl flow is generated near the end of the diffuser. The intensity and flow area coverage of this counter-rotating lateral vortex grows with expansion angle which leads to constant flow area while increasing the expansion angle.

3. When the diffuser length to inlet diameter ratios are between 0.5 and 1.25 the flow provide undisturbed streamline inside the diffuser. By increasing L/D more than 1.25 a separation formed at the end of the diffuser and increase with increasing diffuser length which leads to a constant cross flow area whatever increasing the diffuser length.

4. The flange develop a high pressure region in front of it and low pressure region behind it, the intensity and area coverage of these regions increase with increasing flange height which make a remarkable effect in collection and acceleration of the approaching wind.

5. The greater the flange height, the higher the wind speed and lower pressure at the throat, till flange height to diffuser diameter ratio reaches to 0.75, after that the rate of change of velocity and pressure with flange height is relatively small.

6. By increasing the load factor the acceleration factor decreases until reached to a value of C_t equal to 0.95, at this value the designed diffuser is still effective and able to increase the air velocity passing through it. By increasing C_t more than 0.95 the diffuser will not be effective in increasing the air velocity.

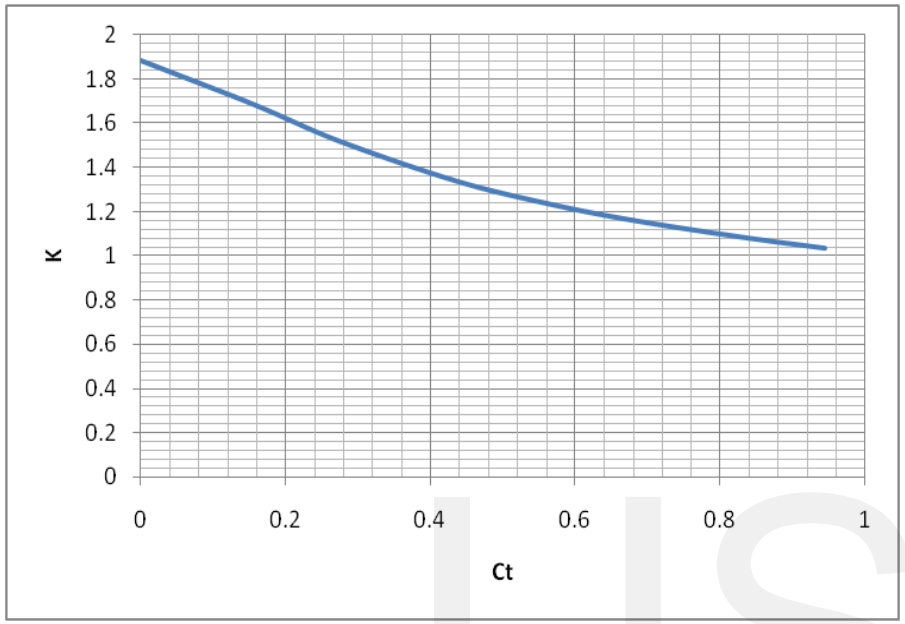

(a)

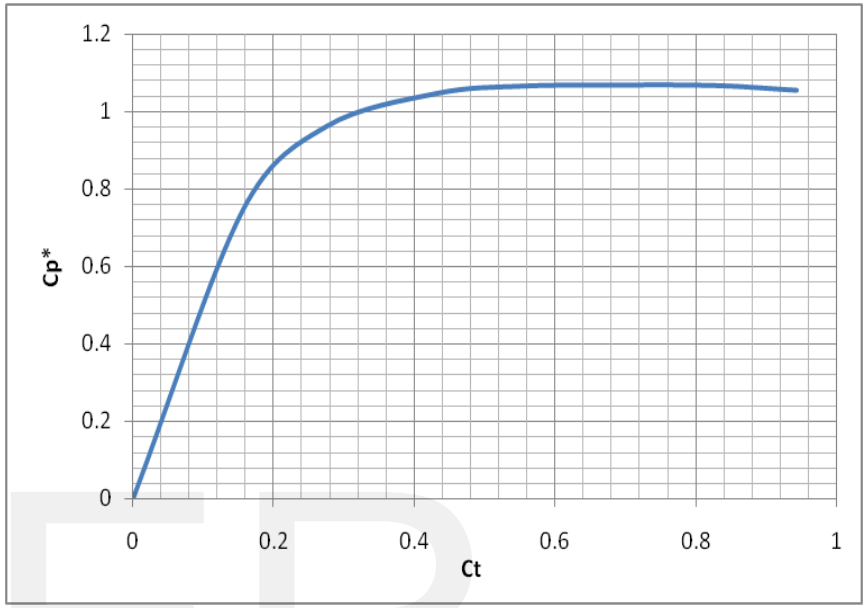

(b)

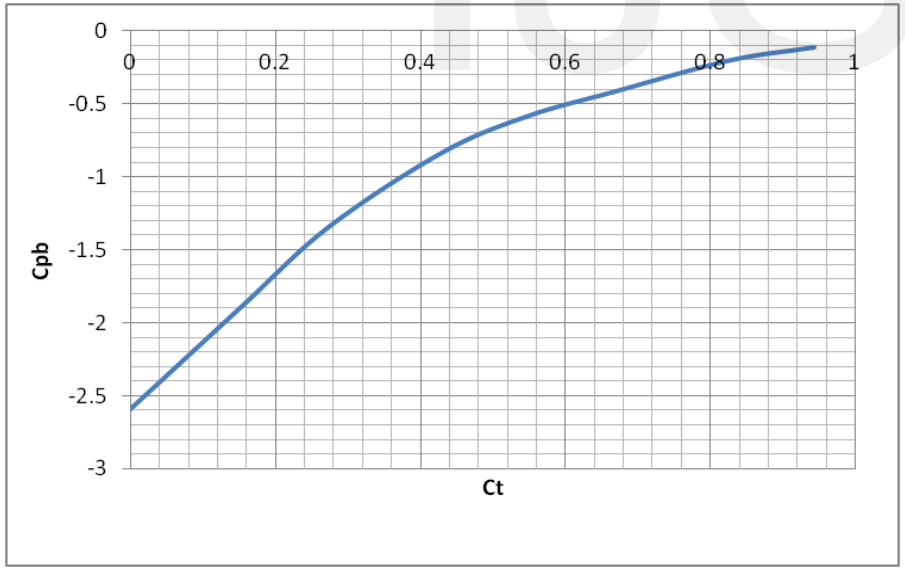

(c)

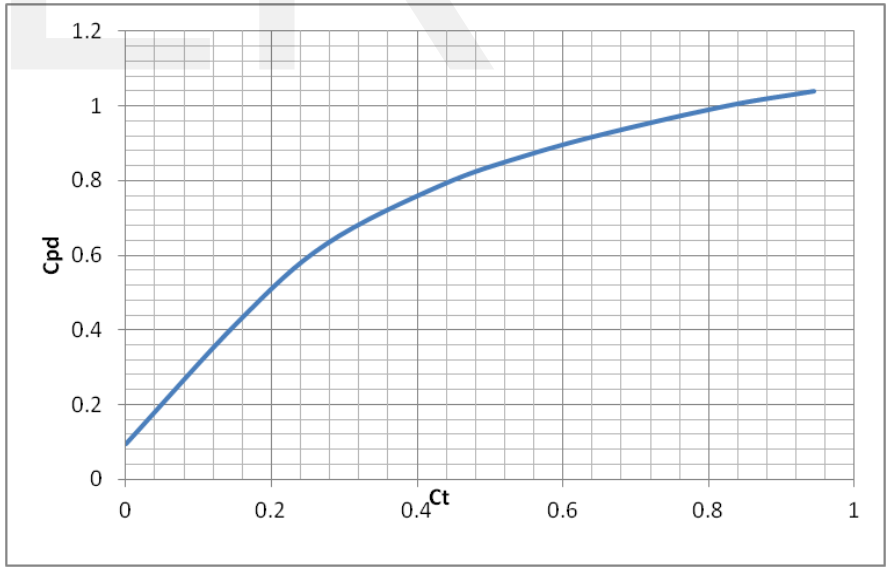

(d)

Fig. 26 Flanged diffuser performance: (a) acceleration factor; (b) input-power coefficient; (c) base-pressure coefficient and (d) pressure-recovery coefficient.

REFERENCES

Abe, K., Ohya , Y. (2004). " An investigation of flow fields around flanged diffusers using CFD," Journal of Wind Engineering and Industrial Aerodynamics, vol. 92, Issues 3–4, March, pp. 315–330

Buyung Kosasih, Andrea Tondelli (2012). "Experimental study of shrouded micro-wind turbine,". Procedia Engineering, vol. 49, pp. 92 – 98

Chen, T.Y. Liao, Y.T., Cheng, C.C. (2012). "Development of small wind turbines for moving vehicles: Effects of flanged diffusers on rotor performance," Experimental Thermal and Fluid Science, vol. 42, pp. 136–142.

Glauert, H. (1959). "The elements of airfoil and airsrew theory,". Cambridge: Cambridge University Press

Kazuhiko Toshimitsu, Hironori Kikugawa, Kohei Sato, Takuya Sato (2012). " Experimental Investigation of Performance of the Wind Turbine with the Flanged-Diffuser Shroud in Sinusoidally Oscillating and Fluctuating Velocity Flows,". Open Journal of Fluid Dynamics, vol. 2, pp. 215-221.

Kardous, M., Chaker, R., Aloui, F., Ben Nasrallah, S. (2013). "On the dependence of an empty flanged diffuser performance on flange height: Numerical simulations and PIV visualizations,". Renewable Energy, vol. 56, pp.123-128.

Kamyar Mansour , Peyman Meskinkhoda (2014). "Computational analysis of flow fields around flanged diffusers," Journal of Wind Engineering and Industrial Aerodynamics, pp. 109–120

Kogan, A. Seginer, A (1963). "Shrouded Aerogenerator Design Study II, Axisymmetrical shroud performance," Department of Aeronautical Engineering, Technion, T.A.E. report 32.

Ohya, Y. Karasudani, T. Sakurai, A. (2002). "Development of high-performance wind turbine with brimmed diffuser," J. Japan Soc. Aeronaut. Space Sci., Vol. 50, pp. 477–482.

Ohya, Y. Karasudani T. , Sakurai, A. Inoue, M. (2004). "Development of high-performance wind turbine with a brimmed-diffuser: Part 2," J. Japan Soc. Aeronaut. Space Sci. vol. 52, pp. 210–213.

Oman RA, Foreman KM.(1975). "Cost effective diffuser augmentation of wind turbine power generators," Grumman aerospace corporation, Bethpage, New york 11714 Second workshop on wind energy conversion systems, Washington, D.C., June 9–11

Phillips, D.G., Flay, R.G.J., Nash, T.A. (1999). "Aerodynamic analysis and monitoring of the Vortec 7 diffuser augmented wind turbine," In: IPENZ Transactions, vol. 26(1), Auckland, New Zealand, pp. 13–19.

Phillips, D.G., Richards, P.J., Flay, R.G.J. (2000). "CFD Modelling and the development of the diffuser augmented wind turbine," In: Proceedings of the Computational Wind Engineering, Birmingham, pp. 189–192.

Toshiaki Setoguchi, Norimasa Shiomi, Kenji Kaneko (2004). "Development of two-way diffuser for fluid energy conversion system," Renewable Energy, vol. 29, pp 1757–1771.

Toshio Matsushima, Shinya Takagi, Seiichi Muroyama (2006). "Characteristics of a highly efficient propeller type small wind turbine with a diffuser,". Renewable Energy, vol. 31, pp. 1343–1354.

Wang, F. Bai, L. Fletcher, J. Whiteford, J. Cullen, D. (2008). "The methodology for aerodynamic study on a small domestic wind turbine with scoop,". Journal of Wind Engineering and Industrial Aerodynamics, vol. 96, pp. 1–24.

Yuji Ohyaa, Takashi Karasudania, Akira Sakuraib, Ken-ichi Abeb, Masahiro Inouec (2008). "Development of a shrouded wind turbine with a flanged diffuser," Journal of Wind Engineering and Industrial Aerodynamics, vol. 96, pp. 524–539.